Biomechanical Texture Coding and Transmission of Texture Information in Rat Whiskers

Dissertation

zur Erlangung des Grades eines

Doktors der Naturwissenschaften

der Mathematisch-Naturwissenschaftlichen Fakultät

und

der Medizinischen Fakultät

der Eberhard-Karls-Universität Tübingen

vorgelegt

von

Maysam Oladazimi
aus Shahrood, Iran

April – 2019

Tag der mündlichen Prüfung: 23.07.2019

Dekan der Math.-Nat. Fakultät: Prof. Dr. W. Rosenstiel

Dekan der Medizinischen Fakultät: Prof. Dr. I. B. Autenrieth

1. Berichterstatter: Prof. Dr. Cornelius Schwarz

2. Berichterstatter: Prof. Dr. Martin Giese

Prüfungskommission:

Prof. Dr. Cornelius Schwarz

Prof. Dr. Martin Giese

Prof. Dr. Uwe Ilg

Prof. Dr. Andreas Bartels

Erklärung / Declaration:

Ich erkläre, dass ich die zur Promotion eingereichte Arbeit mit dem Titel:

“Biomechanical Texture Coding and Transmission of Texture Information in Rat Whiskers “

selbständig verfasst, nur die angegebenen Quellen und Hilfsmittel benutzt und wörtlich oder inhaltlich übernommene Stellen als solche gekennzeichnet habe. Ich versichere an Eides statt, dass diese Angaben wahr sind und dass ich nichts verschwiegen habe. Mir ist bekannt, dass die falsche Abgabe einer Versicherung an Eides statt mit Freiheits-strafe bis zu drei Jahren oder mit Geldstrafe bestraft wird.

I hereby declare that I have produced the work entitled

“Biomechanical Texture Coding and Transmission of Texture Information in Rat Whiskers “,

submitted for the award of a doctorate, on my own (without external help), have used only the sources and aids indicated and have marked passages included from other works, whether verbatim or in content, as such. I swear upon oath that these statements are true and that I have not concealed anything. I am aware that making a false declaration under oath is punishable by a term of imprisonment of up to three years or by a fine.

Tübingen, den ....

Datum / Date Unterschrift /Signature

This thesis is dedicated to Hasti, my parents, and my little sister

For their endless love, support and encouragement

Acknowledgements

I would like to express my deepest appreciation to my supervisor, Prof. Dr. Cornelius Schwarz for supporting me during my research and his enthusiasm and motivation. Dear Conny, working with you was a real pleasure. I learned a lot from you in science and also in life. I always consider this as one of the biggest opportunities of my life.

I would also like to express my sincere gratitude to my PhD advisors Prof. Dr. Martin Giese and Prof. Dr. Christoph Braun for their support, encouragement, and insightful comments.

I would like to extend my thanks to my dear colleagues, Dr. Julian Hofmann, Dr. Arindam Bhattacharjee, Dr. Subhodeep Chakrabarti, Dr. Alia Benali for their guidance and support over the years.

I would like to gratefully acknowledge Graduate Training Centre team and Prof. Dr. Horst Herbert, head of GTC, which during my PhD always I have had their support. Also Dr. Katja Thieltges, administration - finance Coordinator. Many thanks for providing the opportunity to grow through diverse and rich training courses.

Immeasurable appreciation to my dear friends for their moral support. You are great people!

Contents

Summary

Classically, texture discrimination has been thought to be based on ‘global’ codes, i.e. frequency (signal analysis based on Fourier analysis) or intensity (signal analysis based on averaging), which both rely on integration of the vibrotactile signal across time and/or space. Recently, a novel ‘local’ coding scheme based on the waveform of frictional movements, discrete short-lasting kinematic events (i.e. stick-slip movements called slips) has been formulated. In the first part of my study I performed biomechanical measurements of relative movements of a rat vibrissa across sandpapers of different roughness. My major finding is that the classic global codes convey some information about texture identity but are consistently outperformed by the slip-based local code. Moreover, the slip code also surpasses the global ones in coding for active scanning parameters. This is remarkable as it suggests that the slip code would explicitly allow the whisking rat to optimize perception by selecting goal-specific scanning strategies. I therefore provide evidence that short stick-slip events may contribute to the perceptual mechanism by which rodent vibrissa code surface roughness.

In the second part, I studied the biomechanics of how such events are transmitted from tip to follicle where mechano-transduction occurs. For this purpose, ultra-fast videography recording of the entire beam of a plucked rat whisker rubbing across sandpaper was employed. I found that slip events are conveyed almost instantly from tip to follicle while amplifying moments by a factor of about 1000. From these results, I argue that the mechanics of the whisker serve as a passive amplification device that faithfully represents stick-slip events to the neuronal receptors. Using measures of correlation, I moreover found that amongst the kinematic

variables, acceleration portrays dynamic variables (forces) best. The time series of acceleration at the base of the whisker provided a fair proxy to the time series of forces (dynamical variables) acting on the whisker base. Acceleration measurements (easily done via videography) may therefore provide an access to at least the relative amplitude of forces. This may be important for future work in behaving animals, where dynamical variables are notoriously difficult to measure.

Synopsis

Introduction

Fundamental life phenomena are related to information transfer between organisms and their environment. Tactile sensing is one of the oldest information processing systems with vital roles ranging from cell-to-cell communication, via autonomous movement and tactile discrimination to social communication. To explore the external tactile world, two major elaborations have evolved within the epicritic systems of mammals, the orofacial and the paw/hand subsystems. Perhaps the most peculiar orofacial tactile sensors are mystacial vibrissae (also called whiskers). In rodents these are mobile sensor hairs located around the snout. In the evolution of primates, the hand has developed into an elaborate tool for object manipulation, with the consequence that the fingertip has replaced the vibrissa as the most important sensor for active exploration. Both active touch systems are areas of long-standing neuroscientific research: many studies have mapped variables of skin/hair stimulation to response properties of neurons and have thrown reasonable spotlights on the way surfaces are mapped onto the tactile system. I aim to establish a unifying conceptual basis for one of the most highly evolved sensorimotor systems, the epicritic tactile systems in mammals, which affords percepts of object surfaces on the micro- to nanoscale. This study is part of a comparative approach by studying one of the major tactile systems, vibrissae. Rats are highly skilled in discriminating objects and textures by palpatory movements of their vibrissae. I start with asking the question whether task-specific whisking strategies optimize perception.

Since (Mountcastle, LaMotte, & Carli, 1972), researchers have considered frequencies and amplitudes as the most critical features that the neural system encodes, but a paradigm shift has been happening lately. Vibrissa have been introduced as a complex biomechanical tool by

Hartman and Neimark et al.(Hartmann, Johnson, Towal, & Assad, 2003; Neimark, Andermann, Hopfield, & Moore, 2003). These studies were the first to report about resonance phenomena of whiskers, until then biomechanics of vibrissa was hardly investigated. However, the idea that resonant oscillations at whisker-specific frequencies and spatial representations in the brain could be an important tactile cue (Andermann, Ritt, Neimark, & Moore, 2004) has been fraught with many problems, amongst them that resonant frequencies are highly sensitive to boundary conditions like contact with objects. Waiblinger et. al (2015a) showed that not frequency but rather kinematic events (instantaneous amplitude or velocity) are decisive for vibrotactile discrimination. Pulse frequency could barely be discriminated by operantly trained animals while amplitude cues were immediately discriminable. These authors employed a Detection of Change task (DOC) with passive whisker deflections, which showed that the most critical parameter for vibrotactile discrimination is in fact instantaneous kinematic events. These findings drew the attention to the fact that mechanical contact must be understood from the perspective of viscoelasticity and friction, an insight, which has been ignored by major lines of research on tactile perception to date. Tactile sensing involves mechanical contact of integument and touched object. For the fine epicritic tactile sense, these processes critically include the frictional system set up by the conjunction and relative movement of sensor and object. Here, fine frictional movements biomechanically convert a 3D surface texture into spatiotemporal vibration of the integument (hair and skin)(Schwarz, 2016). These processes occur even before the first action potential in a neuron is generated. In this report I focus on rats' vibrissa, sensor hairs that the animals actively move across textures.

Friction packages information about touched textures into movement events of the sensor, called stick-slip movements (or slips for short). In earlier biomechanical studies it had been already shown that fast and jerky kinematic events of duration around 10 ms are regularly evoked and depend on the roughness of the texture (Arabzadeh, Zorzin, & Diamond, 2005; Ritt, Andermann, & Moore, 2008; Wolfe et al., 2008). These events are related to the long-known frictional movements including stick-slip movements that occur in all cases of moving object to object contacts (Schwarz, 2016). These 'slips' as I call them here are due to the biomechanical elasticity of the moving objects. They have been described to occur in machines (Fig. A) that have moving parts, and need to be avoided there, but are also responsible for many natural phenomena displaying rapid displacements (earth quakes due to movement of tectonic plates) or to mechanical systems that emit sounds (squealing noise of hinges, tires on tarmac, singing glasses, violin strings, etc.). Slips are jerky, rare in time, and circumscribed (local in space and time) and occur in a quasi-probabilistic fashion governed by the statistics of the 3D micro-surface rather than its topological outline. Figure A shows the physical model of stick and slip movements consisting in a brick connected to a spring pulled across a frictional surface. All solid objects show brittle as well as elastic characteristics. In the model the first are represented by the brick and the latter by the spring. If a force F is exerted at the spring, it extends and stores the energy that has been applied as long as the brick sticks to the ground. If, however, the force built up exceeds the friction resistance F_f, the brick will suddenly slip across the surface. Certainly, when moving forward, the spring is immediately relaxed and the energy is exhausted. If the pull continues, the jerky slipping process will repeat over and over and generate a saw-tooth-like force trajectory exerted at the brick by the spring and the local peaks in brick

acceleration. An important characteristic is that slips are discrete and temporally local informational events.

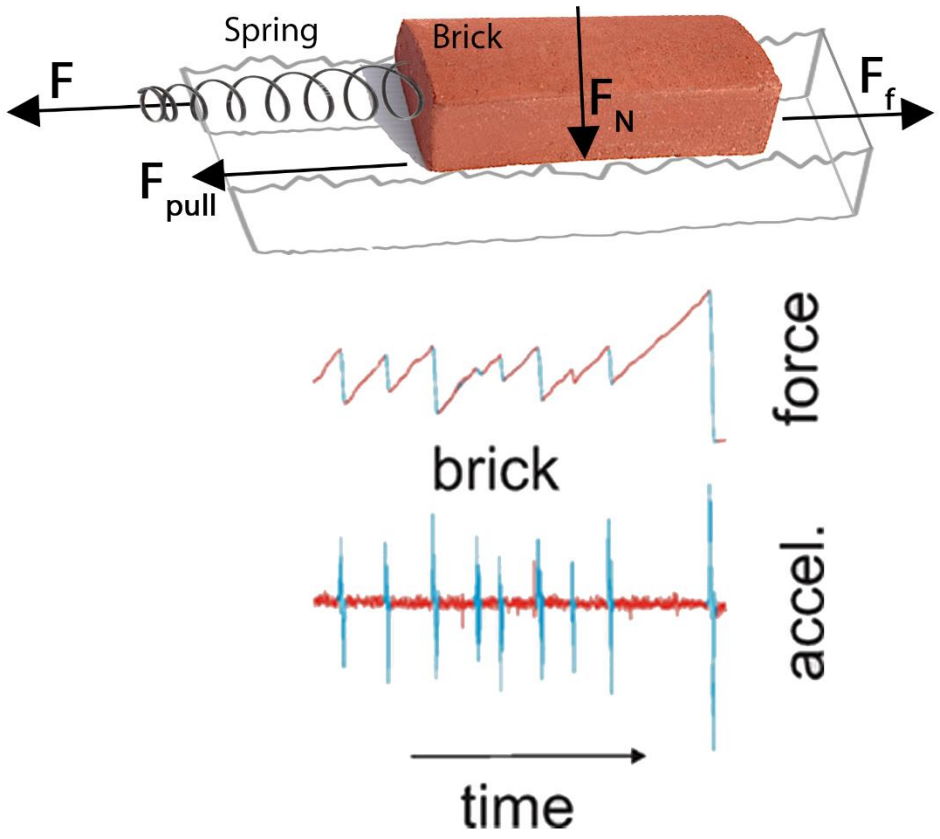

Figure A. Physical model of stick and slip. Elasticity and brittleness of a solid object are modelled by a series of mechanical elements – a spring acting as force transducer, connected to a brick. The normal force (F_N) is the component of a contact force that is perpendicular to the surface that an object contacts and part of the standard model of surface friction is the assumption that

the frictional resistance force between two surfaces is proportional to the normal force pressing them together. A constant force F acting on the spring will extend it and thus increase the force onto the brick until the frictional resistance (F_f) is overcome and the brick sets into brisk motion. This in turn will exhaust the spring-stored energy, bring down F, and stopping brick movement. With continued action of F the process repeats. The force acting on the brick (F_{pull}) across time, thus appears like a sawtooth curve, while the brick acceleration time series shows distinct peaks at the times of brisk movements. These slips are discrete, temporally local events.

The hypothesis I investigated in the present study is that slips might provide the mechanism by which sensory rodent vibrissa code surface roughness. This view has been called the 'Slip Hypothesis' (Schwarz, 2016), and holds that the integument is a computing element that transforms the tactile world in complex ways even before it affects the neuronal tactile receptors. These constraints of tactile perception are likely unique amongst the senses and, if true, must have had significant consequences on the evolution of tactile signal acquisition, transduction, coding and perceptual inference. In the first section of my thesis using biomechanical analysis combined with classification methods from machine learning, I studied whether it is the probability of occurrence and/or the kinematic characteristics of 'slip' events that is the variable to be optimized by active tactile perception. Classically, texture discrimination has been related to 'global' codes, i.e. frequency (signal analysis based on Fourier analysis) or intensity (signal analysis based on averaging), which both rely on integration of the vibrotactile signal across time and/or space. Originally, the idea of global coding has been developed without knowledge of slips. Theoretically, in the absence of frictional movements and slips, coding could directly transform the texture's 2D profile along the 'path' of the vibrissa, e.g. leading to a measurement akin to a contactless distance meter. In reality, however, the conical form (Hires, Pammer, Svoboda, & Golomb, 2013; Towal, Quist, Gopal, Solomon, &

Hartmann, 2011; Voges et al., 2012) and the pronounced elasticity of whiskers (Hartmann et al., 2003; Neimark et al., 2003), inevitably lead to frictional movement and slip generation and renders this simple view unsustainable. Therefore, given the presence of slips, the question arises whether a global code can be considered as optimal to read out texture information contained in slips, or in how far it is able to contribute texture information from other segments of the vibrotactile signal, like oscillations or creepy movements (S. J. Bensmaia & Hollins, 2003; Persson & Volokitin, 2006; Prevost, Scheibert, & Debregeas, 2009). To study this question, I performed the biomechanical measurement of relative movements of a rat vibrissa across sandpapers of different roughness.

There exist previous measurements of vibrations during whisker movement across a texture. However, these studies concentrated on spectral analysis (Hipp et al., 2006), and the occurrence of slips with different roughness (Wolfe et al., 2008), while the dependence of whisker parameters on whisking speed and other movement parameters like distance of involvement with the surface and whisker identity have not been systematically assessed. There is one result presented in passing in a paper by Ritt et al., (Ritt et al., 2008)- but the respective part of the study focused on whisker resonance and oscillations rather than kinematic events. I therefore monitored movement of whisker tips across a surface by high-resolution videography and quantified 1) the roughness of the texture, 2) the distance of the whisker shaft to the texture, and 3) whisker identity (a rat has more than 25 whiskers of different length on its snout), and 4) speed and acceleration of whisker motion across the texture. To vary roughness, sandpapers of different degrees have been used in the literature (Arabzadeh et al., 2005; Hipp et al., 2006; Ritt

et al., 2008; Wolfe et al., 2008), and I adopted this strategy here too. The dependent variables are 1) the probability of a slip per time interval (the rate), 2) slip amplitude, 3) slip speed, and 4) slip acceleration.

Rodent vibrissa are highly elastic hairs (Hartmann et al., 2003; Neimark et al., 2003), which, unlike other cylindrical body hair are conical in shape. Its taper renders a whisker highly pliable, especially toward its thinned end (Hartmann et al., 2003). When brushed up against a pole, the tapered whisker tends to bend easily and can slip straight past, almost immediately. In contrast, a cylindrical hair bends gradually and rubs along the pole until the tip is reached when significant bending energy is released (Hires et al., 2013). The movements employed to strike tactile objects often is rhythmic. This motor strategy, however, can either be overwritten by more complex voluntary motor commands, or can be modulated in its kinematic outlay by the animal (Ranade, Hangya, & Kepecs, 2013). In principle, the animal could choose to vary properties of the whisking motion, such as frequency, amplitude and other parameters in order to optimize its performance in a challenging perceptual context.

In the second section of this thesis, I elucidated the biomechanical principles of how frictional movements transform spatial micro-geometry into spatially and temporally non-continuous slips by studying how such events are transmitted from whisker tip to follicle, where transduction of mechanical signals into electrical neuronal signals occur. To find out about these mechanical mechanisms I again employed ultra-fast videography of a plucked rat whisker rubbed across sandpapers of different grades, this time assessing vibrations along the whole

extent of its shaft. Further, to validate and complete the calculations of moment from kinematic data, I measure the force at the base of the whisker directly. A highly sensitive piezo-resistive force sensor probe that is capable of measuring multiaxial forces in the Micro and Nano Newton range was used to accomplish these measurements. The force sensor measured the normal (F_n) and axial forces (F_a) at the whisker base.

In this thesis I report on using of kinematic data to provide the first detailed biomechanical evidence of how small-scale stick slip motion at the tip is transmitted as force and moment at the whisker base. I will show that the transmission of tip deflections to the base is extremely rapid and serves to greatly amplify the AC component of the moment along the whisker shaft. Thus, in a sense, the whisker is not only a texture transmission device, but it is, in fact a filter and amplifier, enabling small-scale stick-slip motions to be robustly represented at the follicle. The central tenet of my work is that 3D geometry of textures is transformed by a stochastic, non-continuous transfer function implemented by frictional slip movements. This transfer function is thought to realize a biomechanical computation, with two inputs – the perceptional target (the texture) and the perceptual strategy (sensor movements). The output is a discrete, stochastic series of slips, local in time and space. My investigations on the biomechanics of whiskers indicates that slip-based information is superior for texture discrimination.

Results

In the first part of the study, the question to be answered was, how a local encoding variable (like slip acceleration) is related to texture variables (height, slope, angularity), and whether there is a systematic dependence on the contextual parameters (driving speed, distance and whisker identity). Sandpaper profile has been measured through Optical Micro Profilometer for comparison of the surfaces. The first and second spatial derivative of the profile was then calculated, which led to the slope and angularity profile. Results shows that texture variables expectedly reflected sandpaper identity, however, pairwise discriminability differed with all three texture variables. The larger grain size expectedly goes along with greater length of spatial correlation, a parameter estimated from the width at half height of the central peaks in spatial auto-correlograms. The spatial power spectra and their centroids, in contrast, did not show monotonic relationship with grain size. Height was distributed more widely with larger grain size and using height as the discriminanda, only extreme grain sizes could be well discriminated. Using slope and angularity as the discriminanda, the mid ranges of pairs could be well discriminated but discrimination was poor for the extreme grain sizes. The next question that I addressed is whether the discriminability afforded by sandpaper surfaces is reflected by whisker vibrations. Distributions of slip acceleration (sa) obtained with different distances (F, Q, H), and whisker velocities (420, 840, 1260 °/sec) were measured. The results show that sa encodes substantial information from the texture. The largest whiskers reflect the discrimination properties of height distribution and the smaller whisker showed discrimination properties akin of slope and angularity. Slip acceleration encoded textural differences by either in- or decrements. The area under the ROC curve or AUC (In a Receiver Operating Characteristic (ROC)

curve the true positive rate (Sensitivity) is plotted in function of the false positive rate (100-Specificity) for different cut-off points) for all neighboring comparisons of the surfaces based on encoding variables (f, I, sv, sa) was calculated. Results show that discrimination performance based on sa is the best of all parameters. A linear relation between sa and contextual variables was found. The systematic discriminability increases with increase of speed and decrease of distance. Whisker identity reflects discriminability in least systematic ways. Further non-linear classification schemes were applied (support vector machine algorithms with linear and radial basis functions as well as logistic regression) to classify texture based on frequency, intensity, and slip acceleration. Texture information was limited to the part the animal is known to be able to resolve using its perceptual system. Slip acceleration outperformed f- and i-based discriminability, while best performance was seen to be maximal when all 3 variables are provided – leaving room for non-redundant information conveyed by different encoding variables. When the data resolution was reduced to match the perceptual change threshold, the discriminability achieved using f and i variables declined to random performance.

In the second part of the study, I studied how vibrations are transmitted along the whisker beam and how does slip-related kinematic variables relate to dynamical variables. Images from videography over the whisker length across one sweep were analyzed and local curvature was extracted. The results show that whiskers bend in 2nd bending mode, i.e. a movement direction at tip is accompanied with the opposite direction at base. The conduction time from tip to base is ultra-fast – exceeding the resolution of the ultra-fast camara (0.25 ms, ie. frame rate of 4kHz). The 2nd bending mode was a robust finding that was observed independent of the object touched and the presence of oscillations. Next the moment along the whisker was calculated

from the changes of curvature along the beam's length. I found that moment is amplify by 3 oders of magnitude from nN at the tip to the μN range at the base. These results suggest that the taper of the whisker together with its intrinsic curvature may play an important role in determining the range of moments experienced in the follicle and its amplification. Slip-triggered averaging reveals that the moment builds up before the slip and decreases thereafter. To validate the calculations of moment from kinematic data, the force at whisker base during the touch was measured using a chip-based high-sensitive piezoelectric force transducer. Normal (F_n), axial force (F_a) measured that way shows a high correlation to acceleration measured using videography.

Discussion

My results demonstrate that slips contain substantial texture information. The mechanics of the whisker constitutes a passive amplification device that faithfully represents stick-slip events to the neuronal receptors. Tactile processing is a classical field of systems neuroscience and has important technical applications in medicine, robotics and the surface design of consumer goods. The slip hypothesis points to functional explanations of papillary ridges and sensor movement, hitherto almost neglected issues. At last, it would help to combine efforts in two major fields of tactile perception, the whisker field offering exquisite invasive access to molecules, cells and networks and the fingertip field with direct impact on human health and robotics.

The slip code assumes that the tactile percept is based on a non-continuous, high-amplitude signal that can be robustly analyzed almost instantaneously (e.g. by feature extraction or change point analysis). In contrast, the classic 'intensive' coding theory assumes that the tactile percept is a continuous low amplitude signal that needs to be integrated over space-time to prune noise (e.g. by either spectral decomposition or simple averaging (Hartmann et al., 2003; Hires et al., 2013; Neimark et al., 2003)). I have obtained the first detailed spatio-temporal experimental results of stick-slip transmission along a rat's whisker. My results suggest that roughness is related to slips at higher velocity and acceleration, which get faithfully and rapidly transmitted to the follicle. These events cause significant large-movement in both the longitudinal pressure and transverse moment (shear) at the follicle. Interestingly, I find that increased whisking speed has only little effect on the kinematic outline of slips. Instead, it is the roughness of the

sandpaper that appears to affect the amplitude and frequency of stick-slip transitions at the follicle most.

In summary, in the first chapter of this thesis I was able to show that the kinematic profile of slips contains substantial texture information (Oladazimi, Brendel, & Schwarz, 2018). Texture information is converted into series of slip events embedded in noise. Slips relay high rates of texture information and slip code delivers texture information instantaneously – it is a local code (like neuronal spikes). Considering perceptual thresholds, I showed that they are superior to classical parameters 'best frequency' and 'mean speed/power'. I consistently found that slips are susceptible to contextual parameters (whisker ID, speed, distance), allowing the conclusion that individual might choose scanning strategies, optimal for certain perceptual goals, simply by adjusting these parameters.

In the second chapter, I show how slips are transmitted to the follicle and robustly are represented as dynamic variables. These findings support the notion that the biomechanical properties of whiskers are highly suitable to present stick-slip sequences to the ascending neuronal system, and that they may play an important role for tactile perception (Schwarz, 2016). Forces at the follicle can be approximated in relative terms by measurements of acceleration. These results will help to estimate dynamic variables from kinematic measures in experiments with behaving animals in the future.

Slip coding in whiskers have interesting consequences for work in human fingertip. Do slips exist in the ridges of the glabrous skin of the fingertip? And if so, are they used by human's tactile perception?

Ridge also known as friction ridge or epidermal ridge is an elevated slice of the epidermis on the fingers, which are caused by the underlying interface between the dermal papillae of the dermis and the interpapillary pegs of the epidermis in the fingers and toes. These epidermal ridges serve to amplify vibrations triggered from brushing finger across the objects for better transmission of the information to sensory nerves involved in fine texture perception (S. Bensmaia & Hollins, 2005).

Statement of contributions

Paper 1:

Biomechanical Texture Coding in Rat Whiskers

Maysam Oladazimi, Wieland Brendel, Cornelius Schwarz

This is a published paper in Nature Scientific Reports journal (Oladazimi et al., 2018). I performed all experiments and performed all data analysis except the one presented in Figure 7 of the publication. This analysis was designed and run by Wieland Brendel (CIN AG Computational Neuroscience).

Paper 2:

Transmission of texture signals along a rat whisker

Maysam Oladazimi, Kentaro Noda, Isao Shimoyama, Cornelius Schwarz

This is a manuscript in preparation. I performed all experiments and data analysis contained in this manuscript. The measurements using the piezoresistive force sensor were done by myself in the lab of Prof. Shimoyma Tokyo, Japan (Tokyo University) during a 2.5 months visit. Kentaro Noda and Isao Shimoyama have designed and developed this sensor and helped to adapt it to my special purposes. The sensors I employed in the study were produced in the Shimoyama partly before and partly during my stay there. The data collection and analysis was entirely done by me.

The future publication of this material is planned to also contain mathematical modelling done in cooperation with Thibaut Putelat, Robert Szsalai, and Alan Champneys (University Bristol). I contributed to this work, mainly in assuring comparability of data and modeling results, but was not instrumental in designing the mathematical formulation or running the model. As the

modelling work is still ongoing and my contribution has been minor, I did not include it in this thesis.

Chapter 1: Biomechanical Texture Coding in Rat Whiskers

(Oladazimi et al., 2018)

Introduction

The smell of a rose, the colors of a butterfly, or the songs of a calling bird are sensory experiences that arise from neuronal activity after sensory processing has occurred at various levels in the neural pathway. Often the different steps of these neuronal processes are studied in detail. However, the first and very critical step is the sampling of the physical stimulus. This consists in active movements as well as characteristic transduction steps that convert the physical stimulus into electrical activity of sensory receptor cells. such that the stimulus' relevant characteristics (i.e. features) engage the sensory receptor to eventually elicit the appropriate neural responses. Here I study the fine epicritic tactile sense in the rat vibrissal system.

In the current study, I concentrate on the touch of the movable rat's large whiskers on textured surfaces. The relative movement of the sensor (i.e., the whisker) and the texture critically engages the frictional system set up; an interaction that is bound to generate a complex sensory signal because the frictional movement will biomechanically convert the 3D texture surface into spatiotemporal vibrations of the whisker. It is worth noting that this critical step is only the physical interaction between the whisker and the texture, long before the first action potential occurs at the sensory receptor ending (Schwarz, 2016).

Classically, ‘intensity’ and ‘frequency’ have been considered as coding symbols for fine epicritic touch. These coding symbols are calculated by integration of the vibrotactile signal, either in time, space, or both. Hence, these coding symbols can be classified as ‘intensive’ or ‘global’ coding strategies (S. J. Lederman, Loomis, & Williams, 1982; Schwarz, 2016). While intensity results from signal averaging (e.g. mean speed), frequency results from an analysis based on spectral decomposition of the signal (e.g. best frequency).

The mentioned insight that whisker touch with a surface establishes a frictional system gave rise to the suggestion of a new coding symbol – short-lived jerky movements, which in engineering have long been known as ‘stick-slip movements’, and now have been also found in whisker touch– henceforth referred to as ‘slips’(Arabzadeh et al., 2005; Ritt et al., 2008; Wolfe et al., 2008). Slips coding is antithetical to the intensive coding strategy because of the 'local' character of whisker slips with durations of around 10 ms(Wolfe et al., 2008). In contrast to the global coding strategy, the local variety does not require extensive integration in time: immediately after the occurrence and acquisition of a slip event, its features (e.g. maximum velocity or acceleration) can be read out and used by the nervous system (Schwarz, 2016).

Historically, the idea of slip coding was not considered when global coding strategies were proposed (LaMotte & Mountcastle, 1975; Taylor & Lederman, 1975). In the simplest case, global coding may be based on a faithful transformation of the texture profile into whisker deflections - a measure that would be similar to contactless distance estimation. However, whiskers are conical in shape (Hires et al., 2013; Towal et al., 2011; Voges et al., 2012) with pronounced pliability (Hartmann et al., 2003; Neimark et al., 2003) at their thin tips(Hires et al., 2013). Thus, in contrast to the idea of faithful and linear transformation, they have been shown to convert

2D surfaces into a discrete and stochastic slip sequence (Ritt et al., 2008; Wolfe et al., 2008). This said, a global encoding strategy may still be applied, but integration would be across such frictional signals – not across a faithful replica of the surface. Therefore, the question is now how such global coding strategies would fare when tested against a local code that reads in instantaneous slip features. The answer is far from clear as known frictional movements generated by highly elastic material (like e.g. silicones, and rubber - similar in elasticity to hair and skin) sometimes consist in quite complex vibrations, containing not only discrete slips but also oscillations at certain object-dependent frequencies as well as more irregular 'creepy' movements (S. J. BensmaIa & Hollins, 2003; Persson & Volokitin, 2006; Prevost et al., 2009).

Rats' strategy to acquire tactile information goes beyond active sensing, i.e. the movement of sensors to sample more space (e.g. eye movements to bring objects at different locations into retinal focus). Rather they perform what I call 'active scanning'; an active process in the sense that first energy is emitted into the world followed by acquisition of the physical reflections of this energy. Well known active scanning systems are echolocation in bats and whales, and electro sensitivity in weakly electric fish. A typical finding in these systems is that the active scanning part (e.g. the call of a bat,(Jones, Depireux, Simons, & Keller, 2004)) is specifically adapted according to the behavioral goal. Tactile perception – whisker based in rodents but also finger-based in primates – deploys mechanical energy (i.e. sensor movements) and collects back the resulting hair (or skin) deflections and associated torques and forces. These tactile systems have only rarely been investigated with respect to behavioral adaptation to perceptual goals, but the known facts indicate that movement parameters used to touch and perceive the tactile world are far from uniform (Gamzu & Ahissar, 2001). Several movement parameters truly affect

whisker-based active touch and therefore must play a role for tactile perception. Amongst those are, firstly; the distance of the rat's head to the touched object (Quist, Faruqi, & Hartmann, 2011), secondly, the velocity of whisking, and thirdly the identity of the vibrissa(e) used to touch. These contextual parameters will affect the frictional movements i.e. slips rate as well as the slip waveform. Therefore, it is safe to assume that slips besides encoding texture properties of a surface also reflect the scanning strategy of the rat (Fig. 1).

Here I evaluate how global and local coding symbols capture texture properties, and how much behavioral parameters affect the coding. This knowledge will provide initial insights into the feasibility of neuronal predictions of sensory consequences of movement (Bell, 1982), an important concept in motor control (Shadmehr & Mussalvaldi, 2012) required to disentangle textural information from the imprints of active scanning.

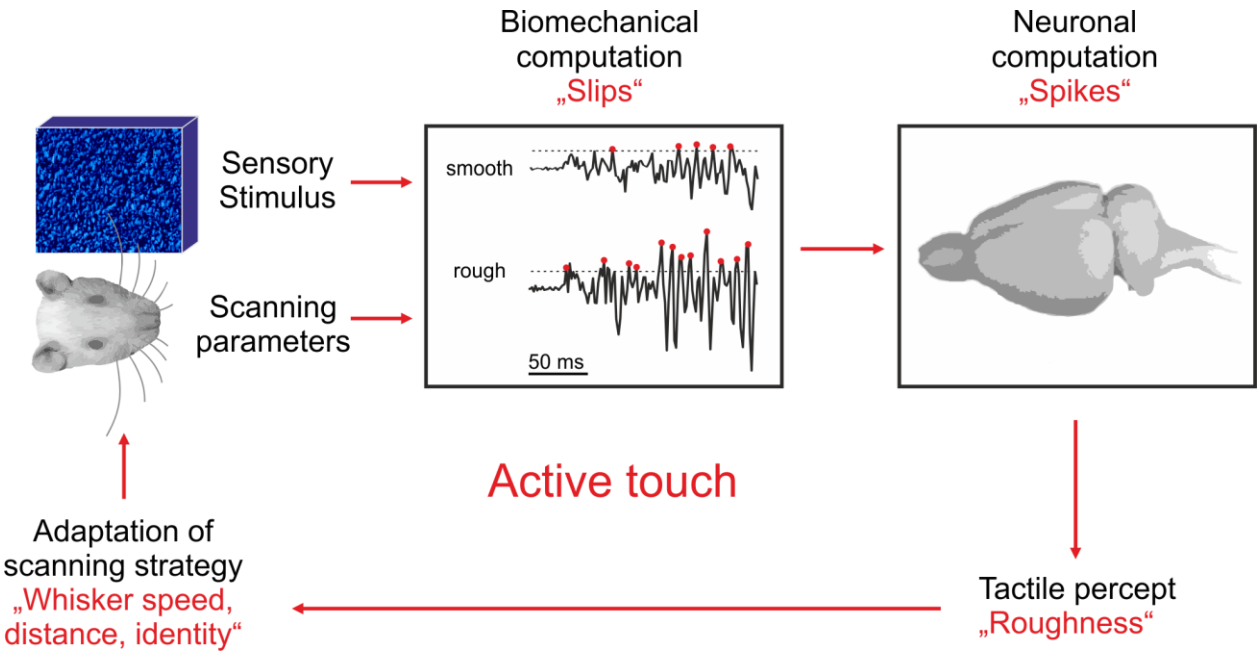

Figure 1. Active touch. The tactile system is an active scanning system. This class of perceptional systems is defined by deployment of energy to the world and sensing the reflections of the deployed energy as a basis for perception. In the case of the whisking rat, the deployed energy consists in kinetic energy, the driving speed with which the whisker is moved across the perceptional target. The sensed reflections of this energy are modulatory movements of the whisker, caused by frictional movement, added to the ego-motion. The modulatory movements are dependent on sensory variables, the texture property, as well as active scanning or contextual variables, amongst them whisker identity, speed, and distance. One instantiation of reflected energy are frictional stick-slip movements ('slips') which are encoded into action potentials in the neuronal system ('spikes'). Whisker vibration and its neuronal representations are therefore the output of a biomechanical computation integrating sensory and contextual variables. This fact allows the brain firstly to read out sensory information, but secondly also allows for a specific adaptation of active scanning strategies to optimize the percept.

Methods

The textures included in this study were a set of 6 different, commercially available, sandpapers (decreasing in roughness) P80, P240, P400, P600, P1200 with the grain diameter of 201, 58.5, 35.0, 25.8, 15.3 µm, respectively (according to the Federation of European Producers of Abrasives). Using an optical micro profilometer (MicroProf, FRT, Germany) I performed 3D profile mapping of the sandpapers surface; this resulted in 6 corresponding profiles, 200 × 200 pixels in size, and 4000^2, 1700^2, 1000^2, 700^2, 500^2 μm^2 in area (following the above-mentioned order). In certain valleys of the 3D profile, the profilometer failed to estimate the correct depth; these errors were highly localized and were constrained within a few pixels. In such cases the device set the erroneous measurements to extreme values, which were easy to identify and separate from instances where the surface approached extreme height by an additional slope criterion [slope in neighboring pixels above 95% percentile]. The bins that included the measurement artifact, along with its neighboring bins, were removed and were linearly interpolated (Fig. 2). The number of pixels, out of 40000, that were removed from each 3D profile were 756, 1158, 829, 844, 2048, respectively.

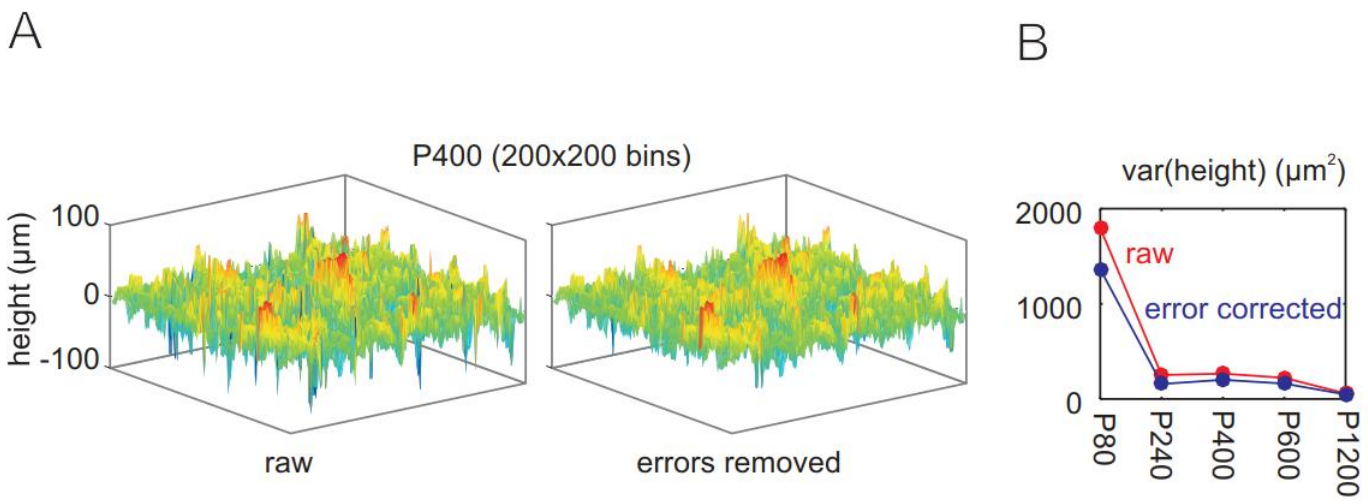

Figure 2. Measurement of sandpaper 3D profile. Sandpapers of different grain size ('roughness', cf. Methods section) were used in this study (p80, p240, p400, p600, p1200). Optical micro-profilometry was used to measure the 3D profile of the sandpapers. Profiles contained errors systematically located at the deepest point of the 3D profile (see the dips in negative height in the 'raw' measurement). These erroneous dips could be easily demarcated, removed and linearly interpolated. The resulting 3D surface after removal of these errors is shown in the center, and its effect on the variance of the height distribution is shown on the right.

I calculated the 'slope' and the 'angularity' as the first and second derivative of the height, respectively (Fig. 3A–C, top). The interpolated values were removed during sampling the distribution (panel 5A). I used a moving window of 2 by 2 bins across the height profile to perform the differentiation. Within each window the difference in the two rows and columns of the profile were assessed by averaging the two differences in each of the directions. The length of the vector sum of the cardinal difference vectors (along row/column) yielded the slope (and angle) within the 2 × 2 window. Using the same procedure on the slope profile I then calculated the angularity profiles. Further spatial power spectra and the autocorrelograms were assessed from the height profiles (Fig. 3D).

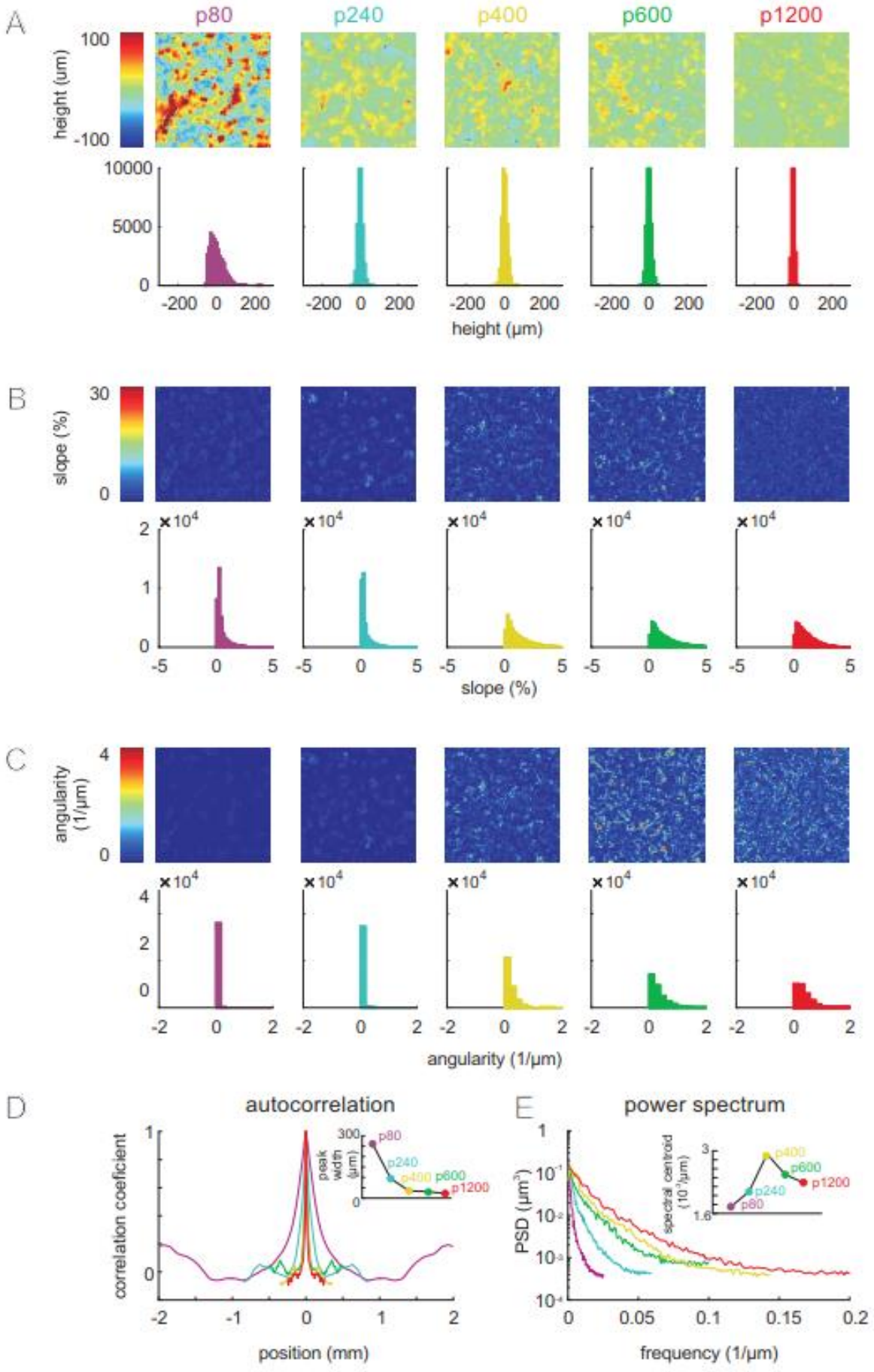
A
p80
p240
p400
p600
p1200
height (um)
100
-100
10000
5000
0
-200 0 200
height (μm)
B
slope (%)
30
0
×10^4
2
1
0
-5 0 5
slope (%)
C
angularity (1/μm)
4
0
×10^4
2
0
-2 0 2
angularity (1/μm)
D
autocorrelation
correlation coeficient
1
0
-2 -1 0 1 2
position (mm)
peak width (μm)
300
0
p80
p240
p400
p600
p1200
E
power spectrum
PSD (μm^3)
1
10^-1
10^-2
10^-3
10^-4
0 0.05 0.1 0.15 0.2
frequency (1/μm)
spectral centroid (10^-3/μm)
3
1.6
p400
p600
p1200
p240
p80

Figure 3. Sandpaper surfaces and characteristic parameter distributions. (A) Measurement of the 3D surface of all five sandpapers (color code is height) and the corresponding height distributions. (B) Same as in A but the first derivative 'slope' is shown. Note that direction of slope is ignored, therefore slope is given in absolute values. (C) Same as A and B, but angularity, the second derivative of height is shown. Again direction is ignored and angularity is given in absolute values. (D) From the grain sizes used to fabricate the sandpapers a monotonic correlation length of height was predicted. I confirmed this expectation by measuring the width at half peak of the central peak of the spatial autocorrelograms calculated from the 3D height profiles. (E) Spatial spectra of the sandpapers. Note that neither the curves nor the spectral centroid reflects the monotonic increment of sandpaper grain sizes.

I carefully plucked 6 whiskers (A2, C2, E2, C4, C6, β) from a single rat (which had been sacrificed after another experiment in our laboratory). I ensured that the hair shaft of the extracted whisker was devoid of kinks, and that the follicle of the whisker was intact. Using microscopic pictures, I digitally measured the length and diameter at the follicle and the tip of the whisker. As previous studies have shown (Towal et al., 2011; Voges et al., 2012), whiskers were almost conical in shape, except for the last few hundreds of microns toward the tip where it tapers irregularly; further the blunt tip usually appears cut and has a width of about 5-10 µm.

Whisker type	Width at the base (μm)	Width at the tip (μm)	Length (mm)
β	190.43	8.72	55.90
C2	184.29	7.42	49.45
E2	178.15	3.59	41.71
A2	162.79	3.07	41.05
C4	124.36	4.61	26.48
C6	81.93	2.05	17.96

I clamped the follicular end of each whisker to the rotational axis of a rod (such that the hair shaft of the whisker stuck out perpendicular to the long axis of the rod, see Fig. 4B); the rod was rotated using a stepper motor (AR66ACD, Orientalmotor, Tokyo, Japan) that was controlled by Built-In Controller Package and data setting software MEXE02, which interfaced via CC05IF-USB to the PC running Windows Operating system. At 50 cm above the rotational plane of the whisker, a high speed camera (MotionBLITZ EoSens® Cube6, Unterschleissheim, Germany) oriented downward filmed the movement of the whisker (camera lens: Tokina 100 mm f/2.8, AT-X PRO – Macro, Kenko Tokina Co.,Ltd., Japan; 160 × 627 pixels, 16 × 16 μm^2/pixel at 4000 fps). I attached the textured surfaces (i.e. sandpapers) to a semi-circular 3D printed (Ultimaker3, Ultimaker, Netherlands) plastic shield such that the center of this circle coincided the rotational axis of the rod (to which the whisker follicle was attached); this ensured that the distance of the follicles to the sandpaper was constant during the rotation.

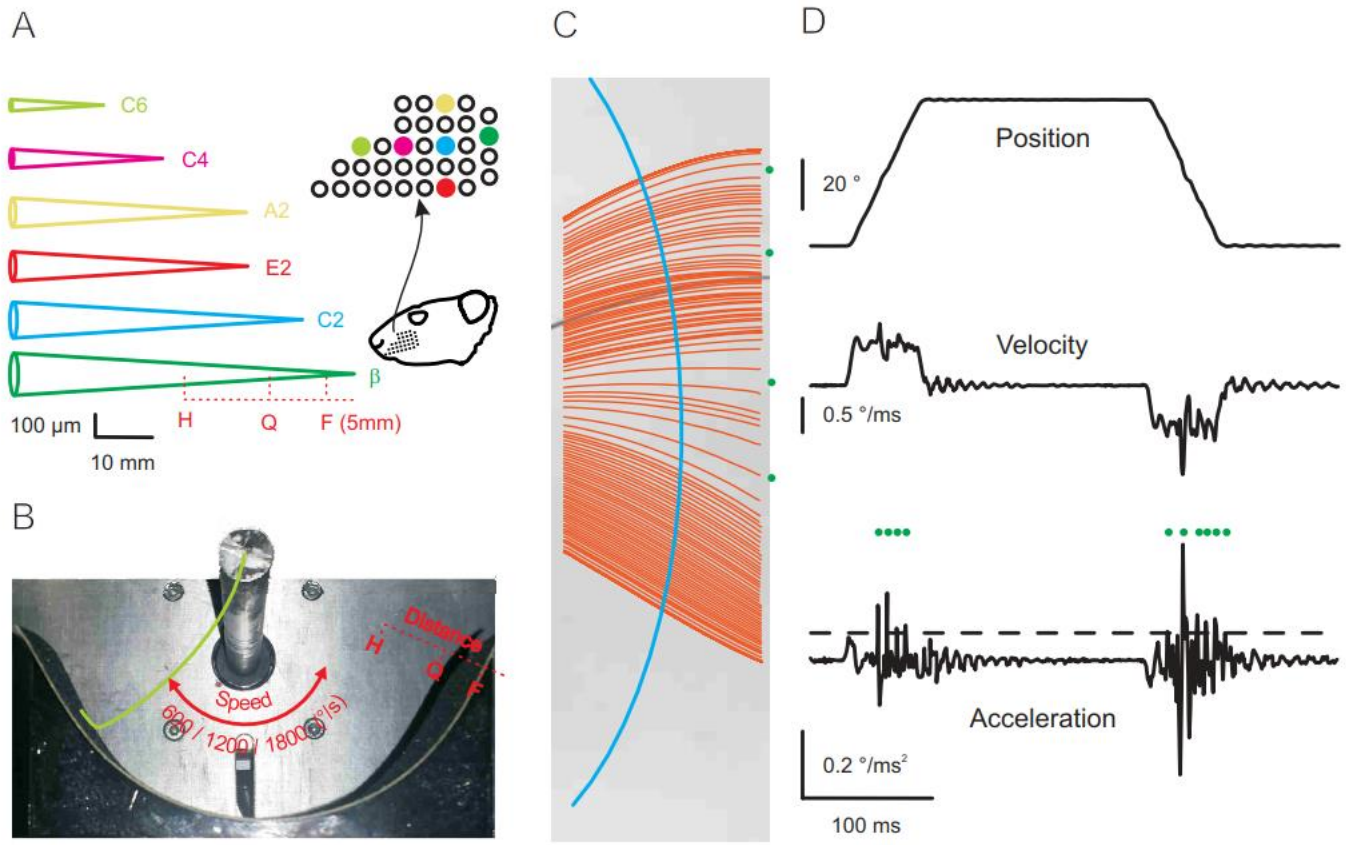

Figure 4. Measurement of frictional movement. (A) Selection of whiskers (names and position on the snout) used for this study. The length and diameters were measured and are depicted as schematized cones on the left (for graphical purposes diameters and length use different scale units; intrinsic bending of the whiskers is ignored). (B) Frictional movement. The rod (top) was rotated by a stepper motor. The whisker (green) was clamped with the follicular end on the rotation axis to the rod and moved at different speeds and distances against the sandpaper carried by the semicircular shield. For the movement of each whisker three shields with diameters adapted to H (half length), Q (three quarter length) and F (total length minus 5 mm) were used (F was not used with whiskers C4 and C6; Q was not used with C6). (C) Example videographic trace of whisker movement. The orange lines depict whisker positions in each frame (4000/s). The blue line indicates the position on the shaft used to extract kinematic traces used in this study (cf. D). Green dots mark the sites at which the whisker acceleration exceeded 2*SD of acceleration measured with movement in air (slips). (D) Position, velocity and acceleration traces extracted from one movement cycle (one protraction). The green dots mark the sites in which the whisker exceeded 2*SD of the acceleration distribution observed with movement in air (using the same driving speed). These events were used to extract slip-related kinematic parameters. As in the majority of retraction movements rotational movements

occurred, this study analyzed exclusively protraction movements (cutting out the first 15 ms after movement start).

The curvature of the 3D printed shields adjusted such that the distance from the follicular base (i.e. the center of the rotating rod) to the sandpaper was equal to 1) the length of the whisker minus 5 mm (F), 2) length of the whisker minus quarter of its length - i.e. three-quarters of whisker length (Q), and 3) half the length of the whisker (H). For one measurement cycle, I performed 60° rotation in forward direction (i.e 'protraction' if it were attached to the rat) against the sandpaper. I specifically ensured that the rotating rod turned in a way so that the whiskers' intrinsic bending (i.e. the curvature of the whisker hair shaft) lay in the plane of the movement direction (see Fig. 4). I implemented 100 measurement cycles for each texture and 100 cycles in free air. During all measurement cycles the hair shaft (at 10mm distally from the rotating rod) were video-recorded; the tip region that engaged with the textures (a small fraction of a millimeter) was ignored as it was obscured by the textural elements.

The whisker movement trajectories were extracted from the videos; an example of one such trajectory instance, a series of whisker shapes acquired from a subset of frames, is shown in figure 4C. Using all the frames for each movement cycle, I reconstructed the whisker position trajectories from which I obtained the velocity and the acceleration traces (i.e. the first and second derivatives of position, respectively, see Fig. 4D). In the acceleration traces, whenever the acceleration (due to brushing against a texture) was above two standard deviations from the acceleration in freely moving whisker in the air (broken line in Fig. 4D), I identified those instances as slips. I also calculated the time of occurrence of each slip event along with the peak velocity and the peak acceleration. To determine the intensive parameters, I calculated the

power spectrum (the maximum of which yields the best frequency) and the mean speed (which is the intensity) for each movement trace. Prior to calculating the power spectrum using Fast-Fourier-Transform, the signal was band-pass filtered (cut off frequencies [30, 250] Hz; Chebyshev type II filter of 5th order) and a Hanning window (raised cosine window) was applied.

I use area under the ROC curve (AUC) as a measure of discriminability of textures in pairwise fashion. AUC is the probability of correct classification of a binary classifier (using varying thresholds to strip off the observer bias) confronted with a randomly picked whisker trajectory obtained with touch on one of the textures (AUC = 0.5 equal to random performance and AUC=0 and 1 equal to perfect discrimination).

I determined the slip-based discriminability using the distribution of 1) peak velocity, 2) peak acceleration, and 3) slip rate. The discrimination of frequencies and intensities were based on distributions of best frequency (obtained by maximizing the power spectra distribution), and mean speed (obtained after subtracting the rotational speed of the motor).

The results from the AUC analysis were confirmed by using three different classifiers (one-against-all) and 10-fold cross-validation (standardized Scikit-learn implementations (version 0.18.151)): 1) Support Vector Machine (SVM) with linear and 2) Radial Basis Function (RBF) kernels and 3) Logistic Regression. To estimate the optimal hyper-parameters for each classifier, the following two steps were performed: first, the data were separated (one whisker/distance/speed) into training and test sets (stratified sampling), and next, a grid-search over the hyper-parameters with a 10-fold stratified cross-validation. The classifier that yielded the best mean cross-validation score was chosen; Fig. 7 shows these scores on the hidden test.

Because tiny differences in frequency as well as intensity can provide texture information (Fig. 7), which are assumed to be clearly below the perceptual threshold of rats (Gerdjikov, Bergner, & Schwarz, 2018; Gerdjikov, Bergner, Stuttgen, Waiblinger, & Schwarz, 2010; Waiblinger, Brugger, Whitmire, Stanley, & Schwarz, 2015), the same analysis was repeated using blurred input data to the classifiers. For perceptual thresholds due to changes in f and i, estimates from previous studies in our laboratory (Chagas et al., 2013; Waiblinger, Brugger, Whitmire, et al., 2015) and from (Manfredi et al., 2014) were used. In previous studies in our laboratory (Chagas et al., 2013; Gerdjikov et al., 2010; Waiblinger, Brugger, & Schwarz, 2015), pulsatile stimuli generated from identical pulses were used (i.e. instantaneous cues from these slip-like deflections could not influence performance). Although there were differences in experimental design as well as stimulus-reward contingencies, 4 rats (Gerdjikov et al., 2010; Waiblinger, Brugger, & Schwarz, 2015) yielded a threshold of ~450 deg/s and ~36 Hz for intensity and frequency differences respectively (cf. experiment 1b and 2b in (Waiblinger, Brugger, Whitmire, et al., 2015), see their Table 1 and Figs 2 and 3). As has been discussed in (Gerdjikov et al., 2018), rats presumably use intensity rather than frequency to generate their percept. Nevertheless, I considered both estimates (of f and i) as a lower bound for the rats' perceptual threshold of change. In (Waiblinger, Brugger, Whitmire, et al., 2015) the authors observed a threshold of 1.14 deg for the change in amplitude of pulses (their experiment 1), which translates to a change threshold of 23600 deg/s^2 in the acceleration domain (cf. Table 1 and Fig. 2 in (Waiblinger, Brugger, Whitmire, et al., 2015)). The reason for repeating the classification analyses using blurred input data to classifier was to demonstrate the effect of excluding texture information below these perceptual limits. To accomplish that each data point was substituted

by a random pick from a Gaussian (with a mean set to the value of the point and standard deviation equaling the respective perceptual threshold); in other runs of the classification procedure the fractions 50% and 30% were used (cf. Fig. 7).

Results

As textured stimuli I used commercially available sandpapers of decreasing grain sizes - p80 (the roughest), p240, p400, p600, p1200 (the smoothest), as done previously in biomechanical and encoding studies (Arabzadeh et al., 2005; Hafner et al., 2003; Hipp et al., 2006). The vibrotactile signals obtained from sandpapers of these grain-sizes has been shown to be behaviorally relevant (Guic-Robles, Valdivieso, & Guajardo, 1989; von Heimendahl, Itskov, Arabzadeh, & Diamond, 2007). I performed 3D profilometry of the textures (Fig. 2) and quantified the height profile, which I next used to determine the slope as well as angularity measures; these measures are the first and second spatial derivatives of height profile, respectively. I ignored the directionality and obtained the absolute values of the measures (units: percent for slope, 1/µm for angularity; see Methods for detailed description, Fig. 3A-C). Spatial correlation of height profiles expressed as width at half height of the central peaks in spatial auto-correlograms point to a meaningful (i.e. monotonic) order with respect to grain size (Fig. 3D). However, it is interesting to note that the spatial power spectra and the centroids extracted from them ('best frequency') did not do so (Fig. 3E).

From a single animal, I plucked 6 whiskers of different lengths (i.e. whisker identity), clamped them individually to the motor shaft, and swept them across the sandpapers that were mounted inside of a cylindrical plane rotated in a circular axis to guarantee constant distance during the movements (Fig. 4A, B). The sweeping movements of the whiskers across the textures were videotaped at 4000 frames per second. For the results presented in this chapter the position traces of one point along the whisker shaft (10mm from the base of the whisker)

was used for further analyses (Fig. 4C, D). Apart from texture identity, three contextual variables were systematically tested as well: I used 6 whisker identities, three driving speeds (600, 1200, 1800°/s; including naturally occurring whisking speeds observed in rats, (Bermejo, Houben, & Zeigler, 1998), and the distance of the follicle to the texture (H: half the whisker length; Q: three quarters of the length; and F: the length 5 mm shorter than the whisker; Fig. 4A, B). Whiskers never come at an exact cone shape. Rather they show a slight intrinsic bending, in which the tip bends backwards to the caudal end of the rat's body. That is, protraction, the forward movement, is executed with the convex side of the whisker leading, whereas retraction, the opposite direction of movement, is performed with the concave side leading. I noticed that the start of retraction is always accompanied by complex rotation movements of the whisker, a phenomenon that occurred much less at the start of the protraction movement. In order to eliminate these complex phenomena, I only considered the protraction movement and ignored the first 15ms of the movement.

I found, confirming earlier studies (Ritt et al., 2008; Wolfe et al., 2008), that the movement was characterized by irregular, jerky movement events, best visible in the velocity and acceleration traces (Fig. 4D). Due to the high pliability of the whisker, the stick-slip movements never showed zero velocity (i.e. an absolute stick phase, Fig. 4D) at least at the measuring point on the whisker shaft. The whisker tip however, was inaccessible for measurement. I therefore took a pragmatic approach to define slips: They were defined as events that exceeded the threshold of two standard deviation of acceleration as measured in freely moving whisker in air (i.e. in the absence of contact and slips; cf. Fig. 4D, acceleration trace). From these slip events, I estimated the peak slip velocity (sv) and peak slip acceleration (sa), as well as slip rate (sr). To determine

intensity (i) I calculated the mean speed and for frequency (f) I identified the frequency that carried the maximum spectral power.

The above-mentioned parameters represent either local or global aspects of whisker vibration in the time domain. The local nature of sa (and sv) enables it to be instantly derived from the vibration trace without any delay or need for integration; intensity, however, is global because to derive it the vibration trace needs to be averaged within a large time interval. As for f, some clarification of terminology is necessary, because previous studies used it in different contexts or estimated it using different strategies. According to my definition, f is the frequency that yields the maximum power spectrum (i.e. the best frequency - this definition is motivated by an earlier study, see (Hipp et al., 2006) . Therefore, using the present definition f is a global variable because power spectra need to be extracted from an extended time interval. This definition needs to be strictly separated from encoding strategies using richer signal aspects. For instance, a recent study by Manfredi et al. (see (Manfredi et al., 2014)), the term 'frequency' incorporated more than one spectral element: the investigators actually used the full power spectrum as the encoding variable. Their definition thus invariably captures global as well as the local signal aspects (see discussion).

Using the highest resolution available in our data, I investigated how well the sandpapers are discriminable biomechanically (Figs 5 and 6). Later I asked, how much of that biomechanical discriminability might be accessed by the rats considering what is known about the perceptual thresholds of these animals (Fig. 7). To accomplish this, I first asked how well 'slip acceleration' (as a local coding variable) is related to texture variables (i.e., height, slope, angularity) and at the same time whether there is a systematic dependence on the contextual parameters (e.g.

driving speed, distance, and whisker identity). I observed, as expected, the texture variables reflected the sandpaper identity (the grain size). However, as observed already before (Fig. 3E) the relationship between the grain size and the different texture variables was not consistent (Fig. 5AB).

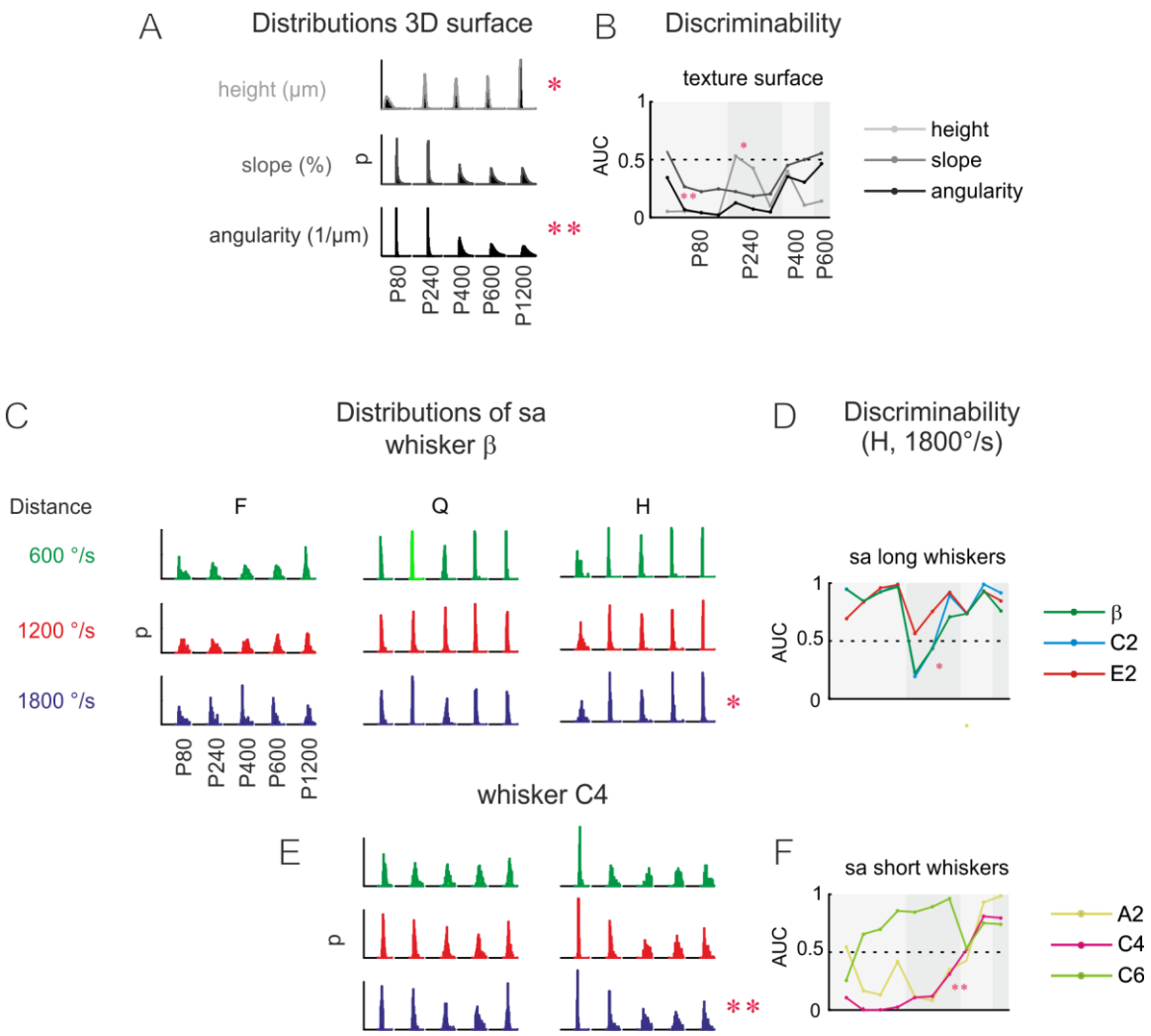

Figure 5. Discriminability of texture and vibrotactile variables. (A) Distributions of variables describing the 3D surface of the sandpapers (height, slope, angularity, cf. Fig. 3). The abscissa holds height (range [−200, 200] µm), slope (range [−5, 5] %), and angularity (range [−1, 1]). The

ordinate holds probability (p, range [0, 0.4]). (B) Discriminability of textures based on texture variables [expressed as area under the ROC curve (AUC)]. (C) Distributions of slip acceleration (sa) obtained with different distances (F,Q,H), and whisker velocities (600, 1200, 1800°/mm^2). The abscissa holds sa (range [−5, 5] 1/mm^2). The ordinate holds probability (p, range [0, 0.4]). Data from whisker β are shown. (D) Discriminability of textures based on sa for long whiskers. The asterisk marks the correspondence with the set of distributions marked the same in C. (E) Same as C but using whisker C4 (note that distance F was not studied with C4 due to its short length). (F) Same as D but plotting the shortest three whiskers. The double asterisk marks the correspondence with the set of distributions marked the same in E. The order of sandpapers as marked in A and C (left) is valid for all blocks of distributions shown in A, C and E. The abscissae in B, D and F hold all ten pairwise comparisons of sandpapers ([P80/P240], [P80/P400], [P80/P600], [P80/P1200], [P240/P400], [P240/P600], [P240/P1200], [P400/P600], [P400/P1200], [P600/P1200]). The striped background marks blocks of comparisons starting with p80, p240, p400, and p600.

While the distribution of height had a broad profile with larger grain size, the distribution widths of slope and angularity decreased monotonically with increasing grain size. Pairwise discriminability turned out to be quite different using the three texture variables (Fig. 5B). Using height as the discriminandum, only extreme grain sizes could be well discriminated. For example some pairs including P80 and P1200 were well discriminable but discriminability was rather poor in mid ranges of pairs. In contrast, using slope and angularity as the discriminanda, the pattern was reverse in some respects: the mid ranges of pairs could be well discriminated but discrimination was poor for the extreme grain sizes (Fig. 5B). In conclusion, each texture variables enables partially good discriminability, though the complexity of the emerging pattern precludes a simple intuitive notion about texture discriminability in general.

After quantifying biomechanical discriminability, I asked whether the discriminability pattern is reflected by the whisker vibrations. In fact, inspecting the distributions some similarities were found. Take for example the sa distributions acquired with whisker β, distance H, and speed of

1800°/s: The distributions seem to reflect those obtained with the height variable (compare the graphs marked by a single asterisk in Fig.5). Similar results were obtained with C2, and E2, i.e. the whiskers of comparable lengths to β. In fact, quantifying discriminability substantiated these impressions: discriminability of height and sa appear to be similar with high values with extreme grain sizes and values closer to random performance in between (Fig. 5D). Interestingly, the smaller whiskers C6, C4, and A2 showed qualitatively different behavior, such that their distributions showed more similarity with those observed with slope and angularity (C4 is exemplified in Fig. 5E, discriminability is shown in Fig. 5F). A distinct characteristics of whisker C6 was that while showing best mid-roughness discrimination like the other small ones, it did so using a sign change of discriminability (AUC > 0.5 instead of AUC < 0.5; Fig. 5F). In summary, these results suggest that slip acceleration is able to encode substantial texture information, albeit in a rather complex format. Non-monotonic, complex relationships of texture variables with encoding variables and corresponding discriminability values became apparent. The groups of large vs. short whiskers related differently to height vs. slope and angularity of textures: The largest whiskers may be able to pick up the discrimination properties provided by height distributions, while smaller whisker may be tuned more toward picking up discrimination properties of slope and angularity. Finally, these data show that dependent on the context, increase and decrease of slip acceleration can encode the same textural differences.

Compared to whisker identity, the other contextual variables, distance and speed, were less distinctive. The next goal was therefore to systematically examine the role of the contextual variables for each coding symbol (f, i, sv, and sa). To this end, I measured discriminability for each variable individually (Fig. 6) and averaged across comparisons of sandpapers with

neighboring grain sizes ([P80, P240], [P240, P400], [P240, P600], [P400, P600], and [P600, P1200]). First, I found that the local (i.e. the slip-based) coding variables yielded highest discriminability. The ranking has sa yielding superior discriminability, followed by sv, anf then the two global variables i, and f. Second, discriminability was affected by whisker identity in complex ways while speed and distance were reflected in different ways. AUC in many cases rises monotonically with increasing speed and decreasing distance – most consistently so with sa as an encoding variable. In summary, amongst encoding variables, the local variable sa provided greatest discriminability as well as highest consistency under varying contextual variables. It is interesting to note that while discriminability based on slip acceleration got better with increasing speed, slip rate declined consistently by 2.65/s on average (see Fig. 6C). Thus, it appears that higher speeds allow for better discriminability based on individual slip waveforms, but it also results in fewer waveforms available for analysis per protraction sweep.

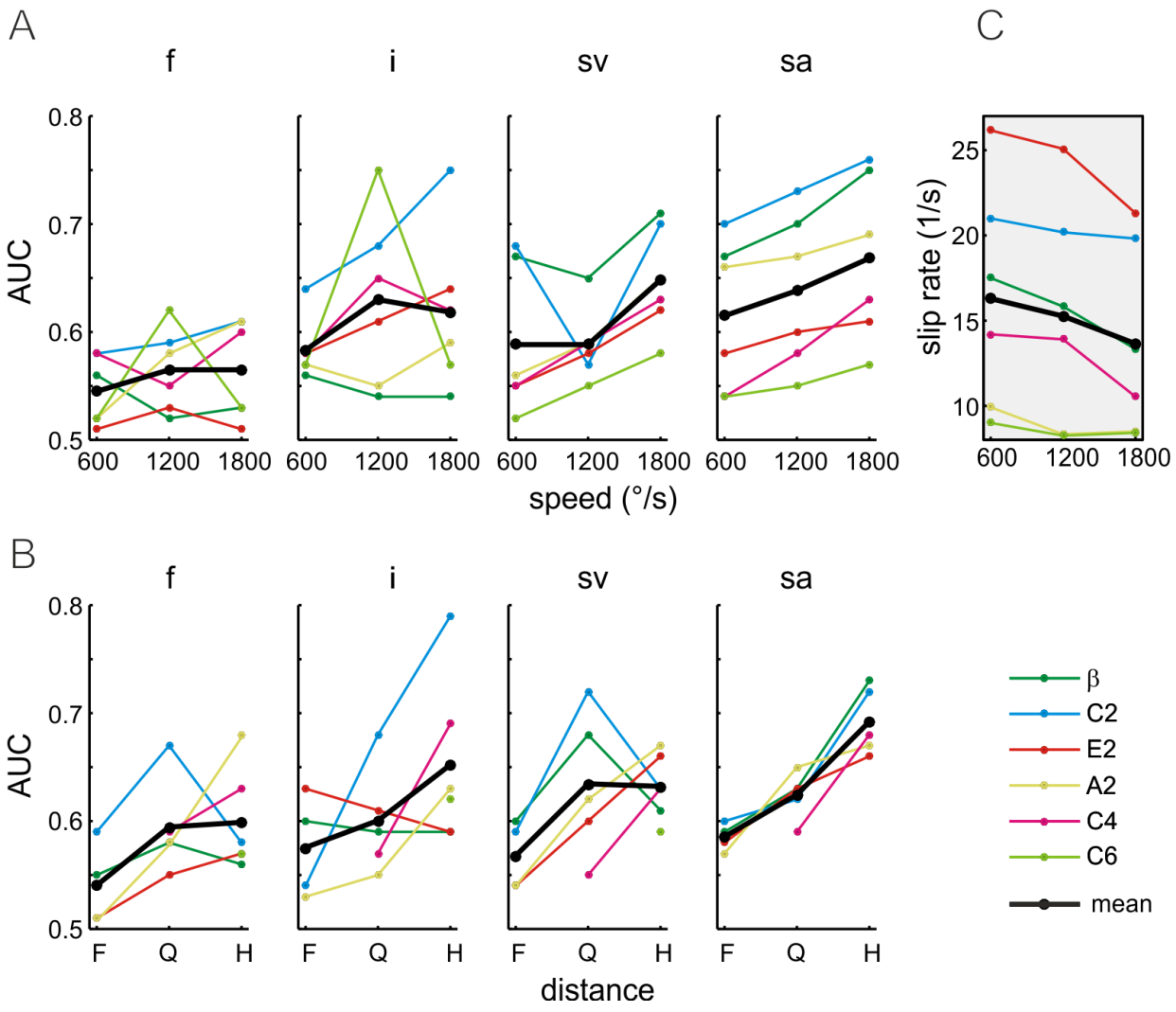

Figure 6. Effect of contextual variables on discriminability. (A) Discriminability and speed. The AUC for all neighboring comparisons ([P80, P240], [P240, P400], [P400, P600], [P600, P1200]) for each whisker (color) and averaged across whiskers (black) is shown based on the encoding variables frequency (f), intensity (i), slip velocity (sv), and acceleration (sa). (B) same as A but for contextual variable distance (F: whisker length minus 5 mm; Q: three quarter whisker length; H: half whisker length). (C) Slip rate observed with the same speeds as in A. The legend is valid for all panels. Note that all encoding variables in this figure were used at high resolution (thus reflecting the biomechanical facts at the maximal resolution provided by our measurements). Please refer to our considerations that texture information may be carried in a range of signal resolution that cannot be used by rats in Fig. 7.

Having seen the contribution of global and local variables in discriminating pairs of textures, I aimed to quantify information in more general terms conveyed by global and local coding symbols. To accomplish that, more sophisticated classification algorithms from machine learning were used: two support vector machine algorithms with linear and radial basis functions as well as logistic regression (Fig. 7). Frequency, intensity, and slip acceleration were used as candidate variables to train the classifiers. Next a 10-fold cross-validation on the training-set was performed to tune each classifier's hyper-parameters, before the classifier that yielded the best cross-validation score was selected. Finally, by determining the median top accuracy of the best classifier on the validation set the final score was found; in other words, the average probability by which the classifier correctly (i) identifies either the texture identity (amongst the 5 possible sandpapers)(Fig. 7A), or (ii) the correct texture when presented pairwise with neighboring grain sizes ([P80, P240], [P240, P400], [P240, P600], [P400, P600], and [P600, P1200]; Fig. 7B). Whereas these analyses may utilize the input variables at a very high resolution, the animals' brains one must take its perceptual limits into consideration. For example, I had measured frequency at a resolution of 1 Hz, a scale that that cannot be resolved by rats' perception and therefore is deemed irrelevant. Therefore, the above-mentioned analysis was repeated with step-wise reduction of the input variables' resolution down to known values of discriminable distances from rat psychophysical experiments (Gerdjikov et al., 2018; Gerdjikov et al., 2010; Waiblinger, Brugger, Whitmire, et al., 2015). Reliable psychometric data from rats are scant and in the cited studies the change thresholds were measured with reference to one fixed value. Therefore, they only provide a starting point to qualify biomechanical discriminability with behavioral constraints. In face of this uncertainty, I decided

to apply a systematic step-wise reduction in input resolution to cover different ranges of input resolution. Input data blurred with a Gaussian that had an SD equal to the change threshold found in the cited studies was assigned a blur of '100%' (cf. Fig 7). Then I repeated the analysis using 30% and 50% filters (i.e. SD equals 0.3 or 0.5 times the respective psychometric threshold), which would provide an intuition about the effect of information if thresholds were lower than reported so far. Further, to ascertain the suitability of slip acceleration as a critical parameter for tactile discrimination, I decided to always reduce its resolution with a blur of 100% (which gave this parameter the most unfavorable condition).

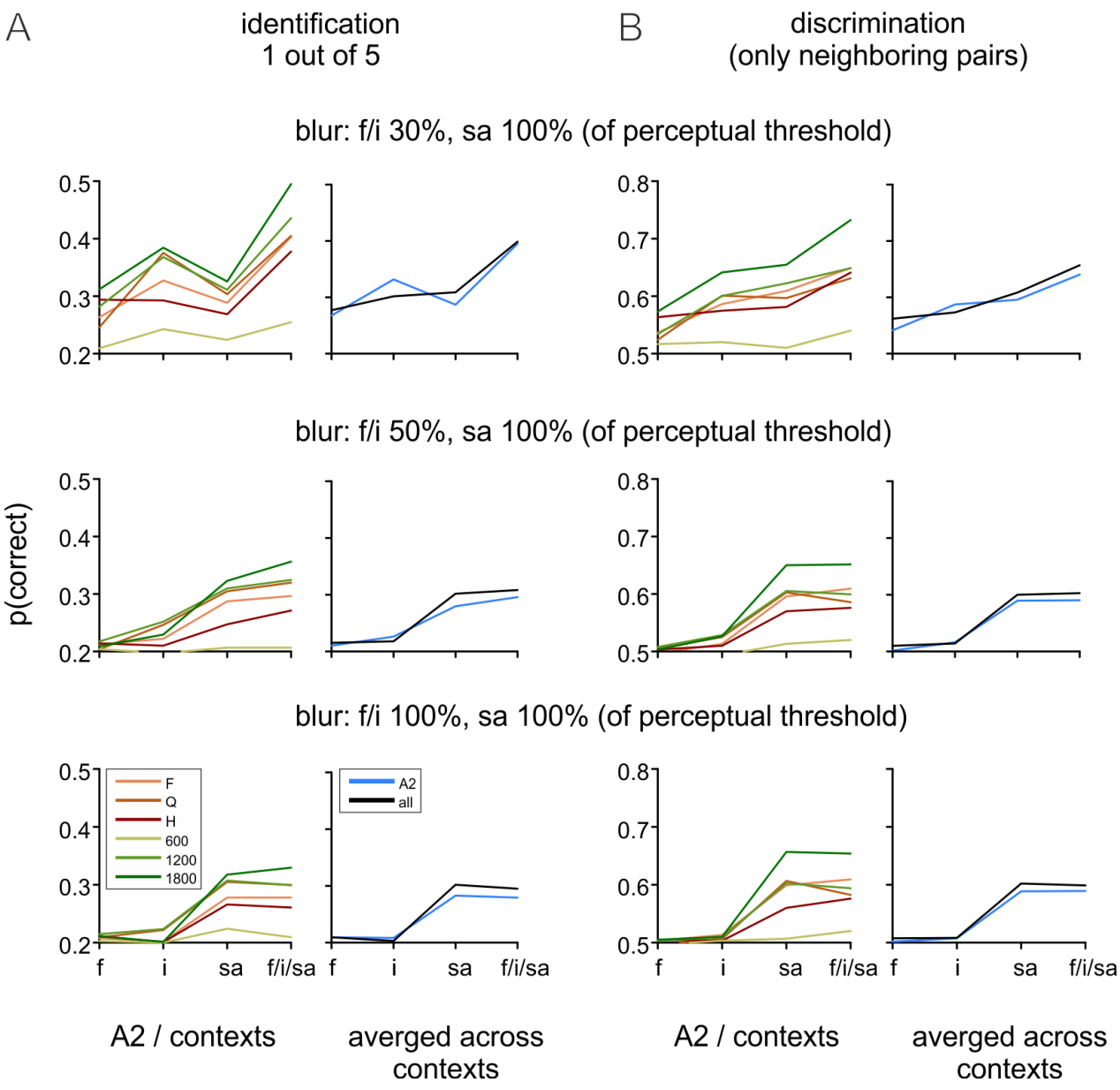

Figure 7. Maximum classification scores obtained from three classifier algorithms using encoding parameters f (frequency), i (intensity), sa (slip acceleration), and f/i/sa (all three). (A) Performance of identifying a texture (out of 5; random performance is p(correct) = 0.2). (B) Average performance discriminating pairs of textures with neighboring grain size ([P80, P240], [P240, P400], [P400, P600], [P600, P1200]; random performance is p(correct) = 0.5). In both panels the left column holds data from whisker A2: red colors depict the performance for different distances averaged across speeds; green colors depict the performance using different whisker speeds averaged across distances. The right column plots averages across all contexts (for whisker A2 and the total sample of whiskers). The rows depict scores obtained with blurring the input data with respect to perceptual thresholds (100%: setting the known change perception threshold as the standard deviation of the Gaussian used to blur the data; 50%, 30%:

setting the standard deviation to 0.5 times the threshold or 0.3 times the threshold; see methods for details). Note that in the top and center rows only the parameters f and i received reduction of blurring. In these rows, f and i are thus favored over parameter sa, which was always blurred at 100%. All plots contain the entry f/i/sa indicating the combined usage of all three parameters as input to the classifiers.

I reasoned that, if under these unfavorable conditions, sa can be shown to provide superior discriminability, it would clearly strengthen the view that it may likely be an important parameter used by perceptual processes. I applied this strategy and observed the following: First, averaged across all 6 whiskers, sa (filtered at 100%) outperformed f and i based discriminability, which was also true for all blurring schemes including the ones that gave f and i a three-fold better chance (i.e. by blurring only by 30%). Second, discriminability provided by the local variables f and i is not redundant and adds to the information available from sa (i.e. the classifier performs best when all 3 variables are provided – cf. the top row of graphs in Fig. 7). Third, degrading data resolution consistently decreased the discriminability conveyed by f and i. In fact, so much so that when the data resolution was reduced to match the perceptual change threshold, the discriminability declined to random performance (cf. columns of graphs in Fig.7; note random performance is 0.2 for the identity task and 0.5 for pairwise discrimination). Fourth, these observations held largely true for inputs stemming from a single as well as from all six whiskers. Fifth, velocity and distance (i.e. the contextual variables) thoroughly affect discriminability, which confirms the more exemplary analyses shown before. It is interesting to note though, that in the case of whisker distance, the AUC classifier shows the best discriminant variable with H distance, while the other classifiers better extract of information contained in slips with longer whisker distances (Q, F).

Discussion

When whiskers brush against textures, which biomechanical variables of the vibrissa movement carry the information for texture discrimination? To investigate this, I specifically compared the local coding scheme (i.e. instantaneous kinematic variables measured from short slip events) against global coding schemes (i.e. the intensive parameters - frequency and intensity). Whereas all coding variables carried enough information to perform texture discrimination, I found that slip acceleration, a local variable, was best for texture discrimination and was most consistent with respect to varying contextual variables (whisker identity, driving speed and distance of texture from the whisker follicle). Although, the global parameters carry texture information, the suitability of these classic global variables are questionable in light of the rats' perceptual abilities.

I used here sandpapers that have been previously used in various other behavioral studies (Arabzadeh et al., 2005; Hipp et al., 2006; Jadhav, Wolfe, & Feldman, 2009; Ritt et al., 2008; Wolfe et al., 2008), which allows us to validate and compare our results to that in the previous studies while restricting the observations to a limited set of real textures. However, a broader investigation will be warranted to determine if and how the results obtained from sandpaper would generalize to a wider range of surfaces. One of the primary dimensions of sorting sandpapers is roughness, which is also a robust perceptual dimension used by humans to characterize tactile experiences. Psychophysical studies in humans suggest that roughness perception is determined by the size of the elemental features (i.e. the wavelength) that constitute a tactile texture (Hollins & Risner, 2000; S. J. J. P. Lederman & Psychophysics, 1974; Skedung et al., 2013; Taylor & Lederman, 1975). Studies that evaluated human similarity

judgments across a wide variety of textures, also reported that roughness consistently appeared in the group of 2 to 3 relevant and independent tactile dimensions (Bergmann Tiest, 2010; Hollins & Risner, 2000; Skedung et al., 2013). Spatial correlation length confirmed the notion that increasing grain size (i.e. roughness) is accompanied by larger wavelength (Fig. 3C). Yet the height distributions and their derivatives (i.e. slope and angularity) did not reflect this monotonic relationship in a simple or consistent manner (Fig. 5B). Presumably, this observation may be due to the fact that the sandpaper surfaces are made up from tightly packed clusters of grains, and that the grain size alone does not exclusively determine the height profile (Fig. 3A). In fact, images (Figure 2.1) taken during the profilometry measurements, show that surface elements are corrugated and vary in size and form, a feature that is expected to enhance the richness of the surface's frequency spectrum. Therefore, local features (i.e. the size and surface of a single grains) are not expected to overly determine the global features (something that might be expected if identical spherical grains are sprinkled sparsely on a flat surface).

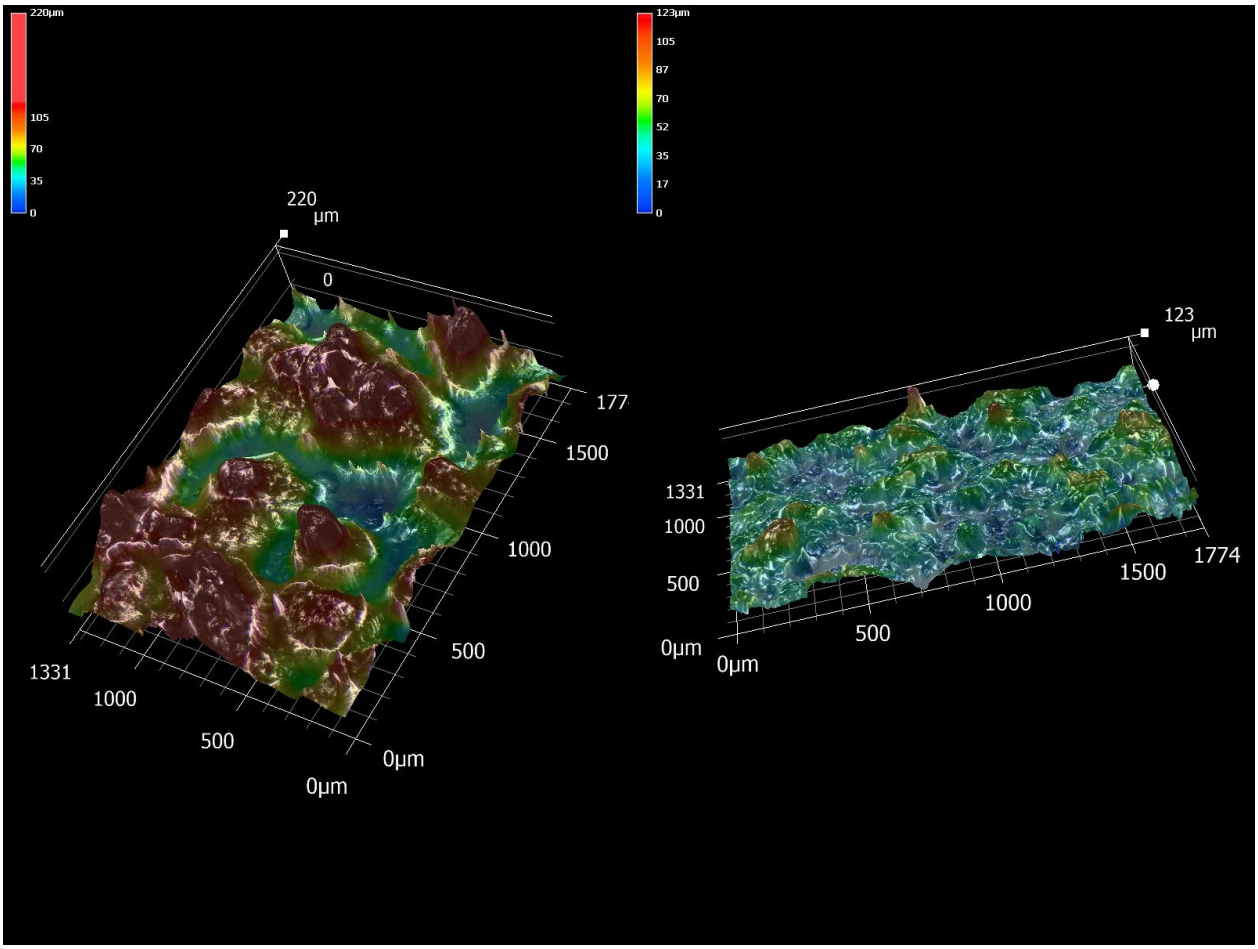

Figure. 2.1. Sandpaper surface profiles measured using a profilometer. Left: P80 sandpaper. Right: P1200 sandpaper.

Another confirmation of this notion was that different surface variables exhibit different and highly complex relationships to texture identity (i.e. grain size, Fig. 5A, B). This in turn questions the plausibility of a simple relationship of roughness with spatial surface variables on one hand and biomechanical variables of the whisker movement on the other. The present findings conform to these doubts - I observed a highly complex reflection of surface properties by the variables characterizing the whisker movement, which was further affected not only by the texture itself but also by the contextual variables (i.e. velocity, distance, and whisker identity, Fig. 5C-F, 6 and 7). As mentioned roughness does play a role for human fingertip-related

perception. My results open the important questions whether roughness should be considered as a valid dimension for whisker based tactile perception. The question related to the human fingertip system is then whether papillary ridges of the fingertip show frictional movement parameters that are better aligned with roughness as the whisker-related ones observed here.

I wish to emphasize that my definition of local variables is in the time domain and not in the frequency domain; i.e. 'frequency' is global in time but local in frequency domain, 'intensity' is global in both time and frequency domain because it is averaged across time or frequency, and finally, 'slip acceleration' is local in time and global in frequency. The clarification of terminology is important as for instance the term 'frequency' has been used in varied way in previous studies (Manfredi et al., 2014; Waiblinger, Brugger, Whitmire, et al., 2015). In this previous formulation the term frequency is quite different from ours, it included a broad array of spectral elements, which presumably included both local and global features in time. Here I show that when classifiers are fed with the combination of cues, i.e. frequency, intensity and slip acceleration variables, the performance gets better in comparison to the performance using any of these features alone. This result extends the finding of Hipp et al. (Hipp et al., 2006) that global variables carry, partly non-redundant, information about the texture, and it provides a biomechanical basis for the fact that if local cues are unavailable, global variables can contribute to the psychometric performance (Gerdjikov et al., 2018; Gerdjikov et al., 2010). I further found evidence that the parametric range of the frequency and intensity variables, that contain relevant texture information might be well below the perceptual threshold of rats (Gerdjikov et al., 2018; Gerdjikov et al., 2010; Waiblinger, Brugger, Whitmire, et al., 2015), a finding that may

serve as a reminder that before identifying the exact mix of encoding variables, it is important to investigate a detailed mapping of the perceptual range.

My results provide quantitative evidence that kinematic profiles of slips could carry texture information, as has been suggested previously (Ritt et al., 2008; Wolfe et al., 2008). Evidence that neurons in the ascending tactile pathway readily encode short kinematic events has been well-corroborated (Arabzadeh et al., 2005; Chagas et al., 2013; Jadhav et al., 2009; Jones et al., 2004; McGuire et al., 2016; Petersen et al., 2008; Pinto, Brumberg, & Simons, 2000; Stuttgen & Schwarz, 2008, 2010; Waiblinger, Brugger, Whitmire, et al., 2015), and there is burgeoning evidence as well that waveform characteristics of slip-like deflections are perceptually relevant (Stuttgen, Ruter, & Schwarz, 2006; Stuttgen & Schwarz, 2010; Taylor & Lederman, 1975; Waiblinger, Brugger, Whitmire, et al., 2015). Psychometric change detection performance of pulsatile ('slip-like') passive whisker deflections is by far superior when local cues are provided as compared to the situation where they are lacking (Waiblinger, Brugger, & Schwarz, 2015; Waiblinger, Brugger, Whitmire, et al., 2015). The present biomechanical results therefore appear as an excellent match to these neuronal and behavioral works.

Which is the decisive kinematic parameter? From the present biomechanical analysis it appears that the encoding of slip acceleration in principle would be superior to velocity encoding to enable texture discrimination. Neurophysiological data is less outspoken. Studies variably suggested the superiority of velocity coding (Petersen et al., 2008; Pinto et al., 2000; Stuttgen et al., 2006) or acceleration coding (Temereanca & Simons, 2003). Low probability spike responses in primary somatosensory cortex to slips have been shown to slip acceleration (Jadhav et al., 2009), while a quantitative encoding study using broadband whisker deflections found that

spike recordings in primary afferents, i.e. the neurons providing and contributing to the end organs attached to the whisker follicle, encodes the position and velocity of the stimulus while acceleration only contributed to a lesser degree (Chagas et al., 2013). Most importantly, paralleling my current findings, the former study found that different kinematic stimulus elements contribute independently to the generation of primary afferents' spikes (Chagas et al., 2013). Therefore, it appears plausible that rats do not perform perceptual judgements based on a single cue, rather their tactile receptor structures have evolved to encode a combination of independent information carried by kinematic variables and thereby optimize their performance.

In the current study, I investigated 3 contextual parameters - whisker identity, driving speed and distance to texture. Whisker identity mapped in most complex ways on the best encoding variable slip acceleration, both local and global (Fig. 6). The data are compatible with the notion that whiskers fall in (at least) two groups: long whiskers might be tuned to the height texture parameter, while the short ones may make use of slope and angularity distributions of the texture. Rats may take advantage of the different biomechanical encoding properties of different whiskers as vibrissal scanning often brings a large subset of whiskers (Bush, Solla, & Hartmann, 2016) in contact with textured surfaces. Nonetheless, future studies will be needed to probe biases of rats to use different whiskers when confronted with different tasks (Waiblinger, Brugger, Whitmire, et al., 2015).

The next contextual variable was the distance - here too noticeable inconsistencies in encoding were present. The finding that information contained in traces measured at different distances depended on the type of classifier (AUC vs. more complex machine learning algorithms) points

to the difficulty to extract texture information independent of distance. It is a fair bet that the rat perceptual system has complex decoding capabilities, and it is therefore a valid expectation that information encoded with varying whisker distances will be accessible by the animals. In any case there can be little doubt that naturally behaving rats are necessarily confronted with the problem to make sense of objects located in different locations with respect to their body. In view of the lack of relevant behavioral data, future studies will be necessary to find out how rats' behavior has been evolved to meet this challenge.

The final contextual variable, driving speed, affected discriminability (both global and local encoding variables) more consistently. Not only did slip acceleration enable highest discriminability, it did so consistently with varying whisking speeds. Assuming the whisker touch yields a signal that is a linear reflection of the 3D geometry of a textured surface, then discrimination based on an intensive variable should be independent of whisker driving speed, because speed merely scales the time series of the incoming signal. This, however, is not the case – neither in the present biomechanical data, nor in perceptual data (available so far only for fingertip movements in humans, cf. (Gamzu & Ahissar, 2001)). Therefore, measurements of global variables are not independent of driving speed, which implies that global variables do not exclusively measure 3D geometry. It is at present most parsimonious to assume that frictional movement, which includes slips and possibly other sub-threshold whisker vibrations, are readily embedded in the signal and thus determine the observed context dependence.

The use of sand paper as stimuli provided rich and near-natural discriminanda, which shows that contextual influence can affect local and global encoding variables. Additionally, it shows that a dominant contribution may be conveyed by contextually specific frictional movements. It

is currently not clear whether the existence of context specificity of encoding is a boon or a bane for texture perception. However, contextual specificity does provide the opportunity to flexibly choose movement strategies when solving tasks in the active tactile perception domain (Carvell & Simons, 1995; Gamzu & Ahissar, 2001). There is a dearth in studies investigating the possibility that frictional processes may determine palpation strategies, a topic that deserves detailed future investigation.

Chapter 2: Transmission of texture signals along a rat whisker

"Manuscript in preparation for submission"

Introduction

Long before neuronal sensory processing takes place, the sensory stimuli, which originate at a distance from the perceiving individual need to travel toward the body and interact with it in some form: either mechanically (touch, auditory), electromagnetic (light) or chemical (olfaction, taste). My topic here, tactile sensing, emerges following mechanical interaction between the integument (hair and/or skin) and the touched object. As the integument moves across the touched object it establishes a frictional system, i.e. a moving contact of two solid objects. Frictional movement involves characteristic stick-slip movements which convert a 3D surface texture profile in a non-obvious and complex way into spatiotemporal vibration of the integument (Schwarz, 2016). Although, there is a strong motivation to study and understand perception as a sensorineural activity or an emergent process of the brain, the mentioned pre-neuronal transformation is often overlooked. In this chapter I would like to use the rat's vibrissa model system to elucidate some core principles of this transformation.

Mammalian whiskers are called vibrissae, as they are vibration sensors (not present in this form in the human skin), which are furnished with an elaborate hair follicle consisting in the bulb and initial shaft of the hair densely packed with blood sinus and multiple nerve endings (Ebara, Kumamoto, Matsuura, Mazurkiewicz, & Rice, 2002). In rats, the so called mystacial vibrissae, located above the snout, are moved by striate muscles and thus can voluntarily be swept across objects. Rodent vibrissae are highly elastic (Hartmann et al., 2003; Neimark et al., 2003), and,

unlike the cylindrical body hair, are conical in shape (Birdwell et al., 2007; Voges et al., 2012). The taper renders the whisker highly pliable, especially toward its thinned end (Hires et al., 2013). The exploratory movement of the whiskers are mostly rhythmic (Welker, Johnson, & Pubols, 1964), a motor strategy, that can be changed by motor commands, or can be modulated in its kinematic outlay by the animal (Gerdjikov et al., 2010; Ranade et al., 2013). In principle, the animal should be able to change the properties of the whisking movement (like frequency and amplitude) to optimize its performance in a challenging perceptual context. However, so far we lack behavioral data that directly address this question.

As I have shown in the first chapter (confirming previous work, Ritt et al., 2008; Wolfe et al., 2008), tracking the vibrissa on the shaft somewhere between the contacting tip to the base (follicle) demonstrates the presence of frictional stick-slip movements (slips). The slips appear as temporally localized features, which, as I showed, hold a substantial amount of information about the texture and are context sensitive (Oladazimi et al., 2018). In addition, by applying system identification methods, studies have revealed that such local features or 'events' are readily encoded on the tactile neural pathway (Arabzadeh et al., 2005; Chagas et al., 2013; Jadhav et al., 2009; Jones et al., 2004; McGuire et al., 2016; Petersen et al., 2008). Finally, behavioral studies have reported that local features decisively determine perception (Waiblinger et al., 2015b, 2015a).

Here I study the question how whiskers vibrate along their entire shaft when they are in contact with a texture on microscopic scale, i.e. with textural elements smaller than a few hundreds of micrometers. This extended view is important to fully understand the relation of frictional movements at the tip of the whiskers to neural coding at the follicle, and eventually perception

(Schwarz, 2016). Specifically, I ask how slip-related kinematic variables (velocity, acceleration) relate to dynamical variables (forces, moments), and how these signals are transmitted along the whisker beam, i.e. from the highly pliable tip down to the much stiffer follicle, where the neural signals are generated. Dynamic variables (like, force and moment) have been suggested to be the critical factors for stimulation of mechanoreceptors at the whisker follicle (Birdwell et al., 2007). However, observations and measurements from the motion of intact whiskers in behaving animals only provide kinematic information. Therefore, I investigated the issue to understand how kinematic variables translate to dynamic variables in the whisker system. I will report that acceleration is highly correlated with force, and consequently, the measurement of acceleration may be a proxy for relative changes of force during a movement.

By using the biomechanical measurements, I provide the first detailed evidence of how slips at the whisker tip are transmitted into measurable forces and moments at the follicular base of the whisker. I show that the transmission of tip deflections to the base is extremely rapid and serves to greatly amplify the AC component of the moment along the whisker shaft. This way slips generated at the tip should be robustly presented to the neurites attached to the whisker's follicle at the base.

Materials and Methods

Experimental protocol

I acquired the experimental data using the same methods as reported in the first part of this thesis (Fig. 8, cf. Fig. 4). Sandpapers of three different grades were used: P80 (rough), P400 and P1200 (smooth), part of the standard series issued by the Federation of European Producers of Abrasives with mean grain diameters of (201, 35.0, 15.3) um, respectively. Two different plastic shields were used, each precision made using a 3D printer of radius that measured 1 or 7 mm less than the whisker's length (Fig. 8A). Hence the distance of the follicle to the textured surface can be varied, although it was held constant for the duration of a particular rotational movement. Our objective was to describe, at a fine-scale, the spatio-temporal behavior of the whisker shaft kinematics as the tip of the whisker made a dynamic contact with the sandpaper. Length and diameter of the whisker and the follicle were measured using pictures taken form a microscope. The whisker is approximately of a conical shape (see also, (Towal et al., 2011; Voges et al., 2012)). In the current study, a C4 whisker (length, l, = 28.36 mm, radius at the base of the whisker = 69 µm) of the rat was used for the experiments (Fig. 8A). The whisker cone appeared truncated close to tip, where it radius was 2.5 µm (Fig. 8B). Also the follicle length was measured to be 1056 µm. As before the whisker was engaged with its convex side first (protraction) and the first 15 ms were omitted to prevent complex pre-steady state movement to enter the data set. Free movement in air was also recorded for reference. I monitored the movement of the free whisker shaft (i.e. from the parts of the tip that was not in contact with the sandpaper to the parts close to the follicle that was not fixed or visually obstructed by the glue and the rod) using a camera mounted above and operated at an ultra-high frame rate (4

kHz;GMCLTR1.3CL-SSF LTR Mikrotron, Unterschleissheim, Germany, 4000 fps, 480x270 Pixels; Tokina objective). The camera was positioned above the rotational plane of the whisker in order to record this planar motion.

For the present analysis stick-slip movements were subdivided in a sticking and a slipping phase. Sticking timestamps, marked as red dots in figure 8D, were defined as the minimum velocity below a threshold of 420 °/s (measured on the shaft 3 mm from the base). This threshold was set arbitrarily, as due to the elasticity of the whisker, velocity along the beam never reached zero. As before, slip timestamps were defined as times of maximum acceleration above a threshold of 2*SD of acceleration values measured with movement in air. Figure 8E shows a kinematogram of whisker movement with stick and slip timestamps marked by their respective colors. The alternating sequence of stick-slip events can be appreciated. Throughout the text, I will refer to these two event classes as 'sticks' and 'slips'. I further measured the shaft curvature and moments at all points along whisker length.

The forces at the base of the whisker were measured using a custom made piezo-resistive force sensor probe, capable of measuring multiaxial forces in the Micro- and Nano-Newton range (Fig. 12A) ((Kan et al., 2013)). The whisker follicle was glued on top of the measuring probe of the sensor. As any movement of the fragile sensor was prohibitive, the sensor (plus glued whisker) was kept still. Instead, the sandpaper was mounted on a rotating drum facing and in contact with the whisker tip, and moved on a circular path centered on the whiskers follicle (Fig. 12A). In this setting the force sensor measured the normal force (F_n) and axial force (Fa) at the whisker base with the resolution of 100 kH. To capture the kinematics near the stiff base of the whisker I used a higher frame rate for the videography (9600 fps; cf. Fig. 9; a_x, red in Fig. 12).

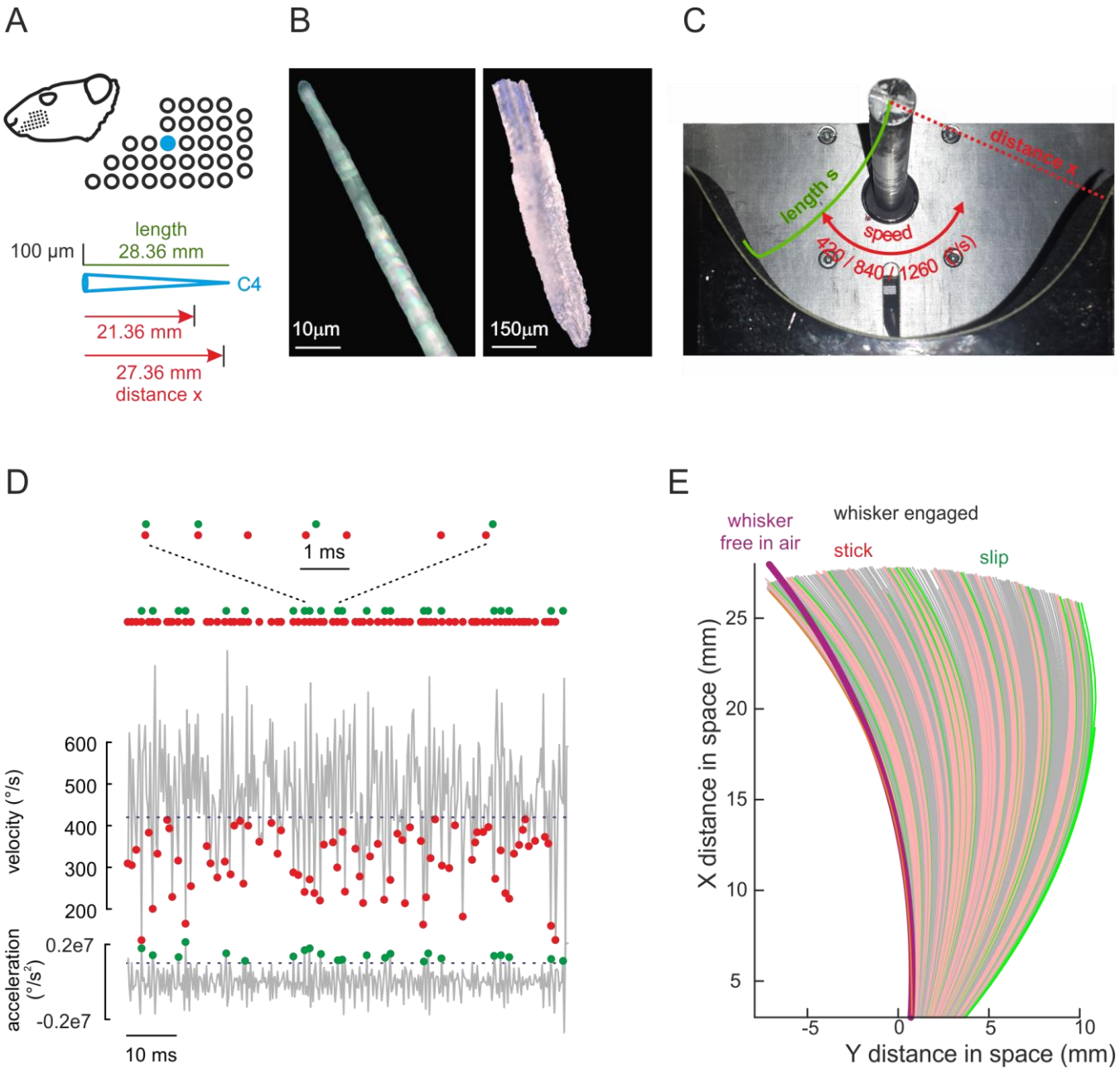

Figure 8. Biomechanical measurements. A) Rat whisker C4. The rat's head and location of whisker field is shown. The position of C4 is marked in blue in the magnified field. Conical shape, length and distance (cf. panel C) are shown. B) Microscopic images of whisker tip (left) and base (right). C) Experimental set up (view roughly like the one of the recording camera). Measurements of whisker length s, driving speed, and distance x are indicated. The rotating rod is seen on top. At the bottom the half-cylinder holding the sandpaper is shown. D) Sticks (red) were found by thresholding the velocity trace at 420 °/s (the driving speed in this case) and minimizing the trace below that limit. Slips were found by maximizing the acceleration strips above threshold (2*SD found with movement in air/no contact). E) Whisker shape and location during one protraction (all frames of the video). Red: sticks (here all frames below the velocity

threshold have been colored). Green: slips. The whisker not engaged on a texture (free in air) is also shown for comparison.

Data analysis

A bespoke algorithm coded in Matlab based on image contrast was employed to track the position of the whisker at each frame. Time series of movements of discrete points along the whisker beam in space were recorded. The resolution of whisker tracking along the whisker length was 48 µm. The position time series was assumed to correspond to the position coordinates of the centerline of the whisker at each instance of time. The data at each time step was used to compute an arc-length coordinate *s* and the signed curvature at each material point along the whisker, respectively given by

$$s = \int_{x_0}^{x} \sqrt{1 + (dy/dx)^2}\, dx, \qquad \kappa = x'(s)y''(s) - y'(s)x''(s)$$

where the prime refers to the derivative with respect to the arc-length *s,* x, x_0 are the start and end of *s* coordinate. For consistency, with the model, I assumed the inextensibility of the whisker. Note that, as the spatial sampling frequency varied slightly from one frame to another (mostly due to loss of data points near the whisker's tip), I used spline interpolation (via the Matlab function interp1) to form a regular spaced grid of the arc-length from the raw data, imposing an arc-length increment of ds. The trajectory of any material point labeled by its arc-length coordinate can then be read out from these interpolated arrays $(x(s,t), y(s,t))$. Figure 8 shows a series of whisker shapes obtained using this method. I also monitored the time series

of the position angle $\psi(s,t) \coloneqq tan^{-1}[y(s,t)/x(s,t)]$. Correspondingly the angular velocity signal $\psi(s,t)$ is obtained from the numerical time derivative of $\psi(t)$. Subtracting the solid rotation of the whisker, I finally derive the rotation fluctuations kinematic variables $\tilde{\psi} = \psi - \Omega_{shaft}t$ and $\tilde{\psi} = \dot{\psi} - \Omega_{shaft}$.

Results

Speed of mechanical wave along the whisker

To estimate the speed of biomechanical conductance of a slip from the whisker tip to its base, I investigated the acceleration near the tip ($a_x(s = 24mm)$) and near the base ($a_x(s = 3mm)$), during one whisker protraction in touch with the sandpaper (P80 and P1200) and calculated their cross correlation (Fig. 9). Acceleration traces sampled with P80 (rough sandpaper) and P1200 (smooth sandpaper) readily showed slip events. They are more prominent when the whisker is in close contact with the surface (7mm of the tip of the whisker engaged with the surface rather that 1 mm of the tip), and when they engaged with the rough surface rather than the smooth surface (Oladazimi et al., 2018). It is noteworthy that, as will be reported in detail in the next section, the whisker oscillates in second bending mode. Thus tip and base bend in the opposite direction, a fact the negative correlation coefficient at time lag zero bears out nicely. The largest absolute correlation was observed exactly at time lag zero, which indicate that the speed of the transmission from tip to the base even exceeded the resolution of our fast videography (4 kHz). In other words a slip at the tip is reflected by a corresponding negative deflection at the base almost instantly – within less than 0.25 ms.

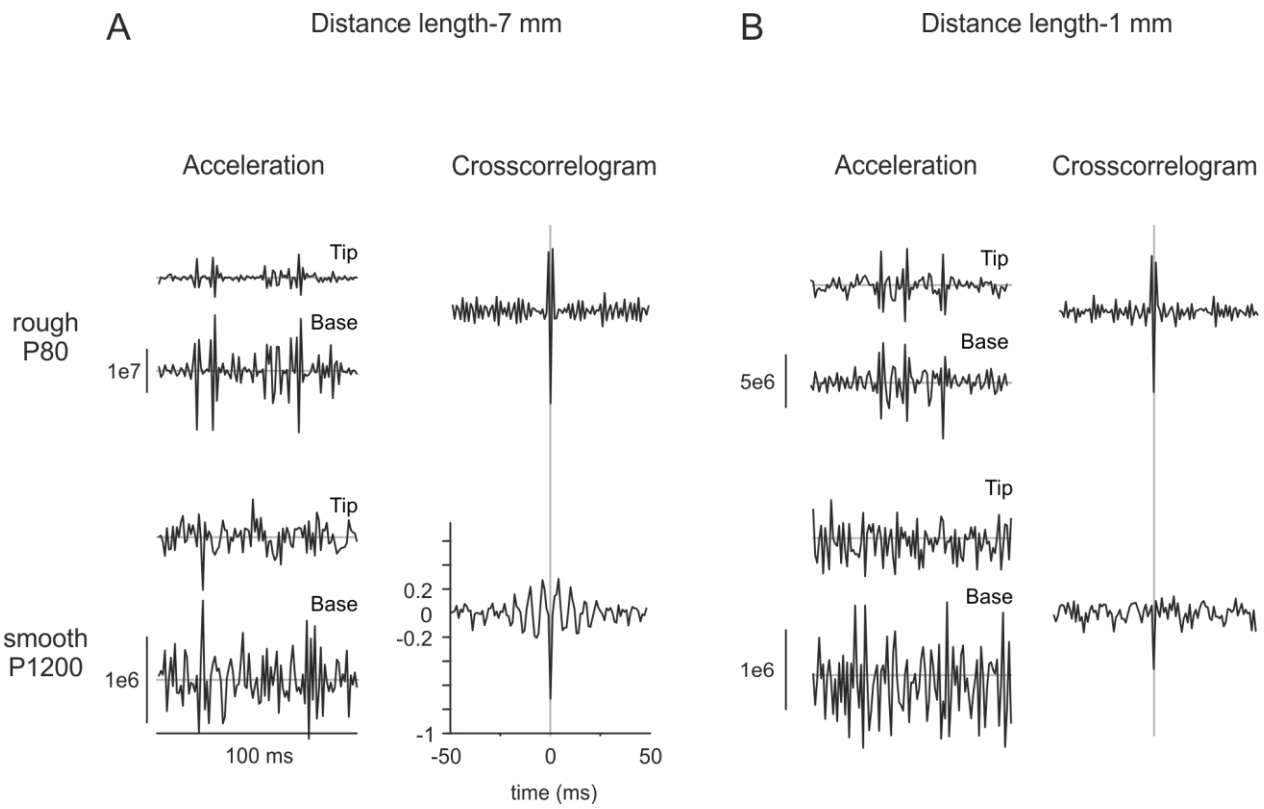

Figure 9. Speed of conveyance along the whisker beam. A) Moving contact using distance of whisker length minus 7 mm. B) Same using distance of whisker length minus 1 mm. In both panels the contact with the rough p80 sandpaper is shown at the top, contact with smooth p1200 sandpaper is at the bottom. On the left column's acceleration traces measured at the tip 25 mm and base 5 mm are shown. The right columns show mean cross-correlograms calculated form all trials measured in this configuration. All negative peaks are located exactly at time delay 0 (vertical gray line).

Whiskers vibrate in the second bending mode

When the whisker makes contact with textures, the whisker tip and base deflect opposite to each other. To study this phenomenon along the entire shaft, I calculated the curvature based on the measured kinematic data by determining the angle θ spanned by the vector orthogonal to whisker base and the tangential force acting along the whisker beam (Fig. 10A inset). Curvature κ is defined by the spatial derivative of θ ($\kappa(s) = \dot{\theta(s)}$). I plot curvature $\Delta\kappa = \kappa_i - \kappa$

(with κ_i being the intrinsic curvature) at all points along the shaft across time (Fig. 10). When moving in air, the whisker oscillated between roughly its intrinsic shape ($\Delta\kappa = 0$; arrow heads in Fig. 10A-B), and a deflection with the tip curving backward ($\Delta\kappa(tip) > 0$) and the base curving forward ($\Delta\kappa(base) < 0$; between arrow heads), corresponding to an oscillation in the second bending mode. The result was an opposite change of curvature relative to the intrinsic shape with the node located on the beam, at about 8 mm distance from the follicle (the node is defined as $\Delta\kappa = 0$). The oscillation frequency was close to 200 Hz (Fig. 10A).

Once the whisker was in contact with a surface the curvature at the tip changed to forward direction ($\Delta\kappa(tip) < 0$) as expected (indicated by the blue color around the whisker tip at $s \cong 24\,mm$ in panels B-E of Fig. 10). In the case the whisker moved over a smooth surface at far distance ($x = l - 1mm$, Fig. 10B), the engagement with the surface dampened the free vibrations of the whisker, but it was still partially detectable and occurred at the same frequency as seen in the free-in-air condition. In addition, a second spatiotemporal structure of vibration became visible: sharply demarcated vertical stripes at irregular intervals corresponding to slips running down the beam at ultra-fast pace (examples are marked by arrows in Fig. 10B). Rougher sandpaper (Fig. 10C) and closer distance (10DE) extinguished the 200 Hz oscillations completely, and only the sharp slip events remain visible. In all these situations, the second bending mode holds, with the node shifting toward the base of the whisker with increasing tip engagement (i.e. shorter distance or rougher sandpaper). Therefore, the second bending mode is a robust feature for resonant oscillations in air as well as non-rhythmic vibrations when in contact with a surface. Figure 10F shows the spectra of the whisker vibration for the larger distance. The second harmonic of the oscillation featured prominently during free in the air

movement (green) and when the whisker engages with the smooth P1200 sandpaper (blue). It broke down when the whisker engaged with the rough P80 sandpaper (red).

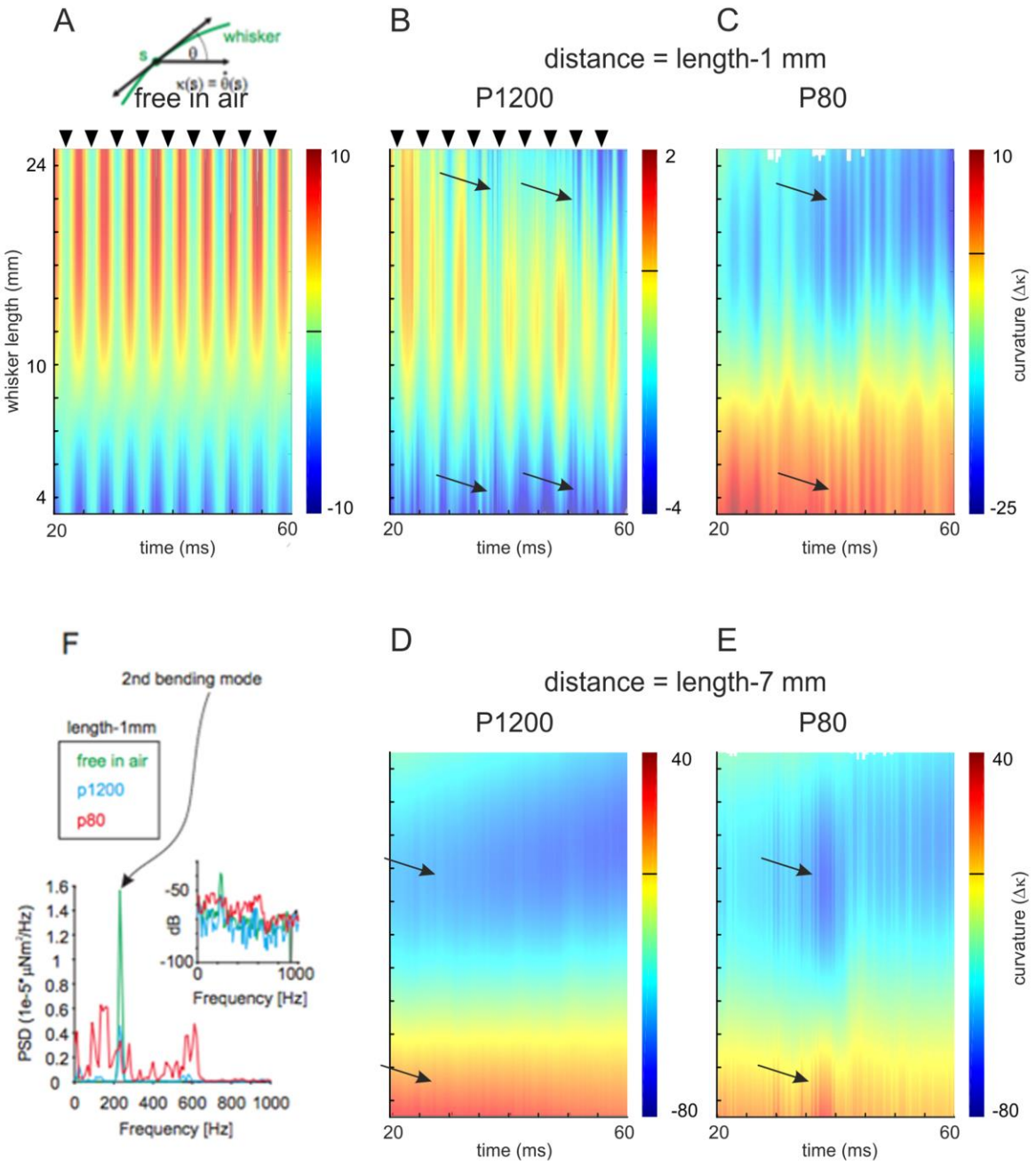

Figure 10. Whisker curvature ($\Delta\kappa$) at all points along length s and trial time. Intrinsic curvature (κi) has been subtracted. A) Movement without texture (free in air). Strong resonant oscillations at 200 Hz (triangles mark periods) dominate the picture. Note that at the time of triangles the

whisker roughly assumes $\Delta\kappa$ =0 i.e. the intrinsic shape. B) Movement in contact with P1200. Distance = length minus 1 mm. Triangles mark remaining resonant oscillations. C) Same as B but contact with P80. DE) Same as BC but distance = length minus 7 mm. F) The spectra of the whisker vibration for the larger distance. The second harmonic of the oscillation featured prominently during free in the air movement (green) and when the whisker engages with the smooth P1200 sandpaper (blue). it broke down when the whisker engaged with the rough P80 sandpaper (red).

Amplification of moment from tip to base

The moment $\mathrm{M_{na}(s,t)}$, related to rotatory forces at each point s of the shaft in the plane of movement can be estimated knowing the curvature at this point and time t (spanned by the normal force F_n and the axial force F_a; inset in Fig. 11B). $\mathrm{M_{na}}$ is calculated as follows:

$$I(s) = \frac{\pi}{4} r(s)^4 \qquad (eq.1)$$

$$M_{na}(s,t) = EI(s)[\kappa(s,t) - \kappa_i(s)], \qquad (eq.2)$$

where 'I' is the second moment of the circular cross section at point s along the shaft (eq. 1 plugged into eq. 2), E is the Young modulus, κ is the measured curvature, and κ_i is the intrinsic curvature (Fig. 11A).

Calculating and plotting $\mathrm{M_{na}}$ reveals that a small moment at the tip of the whisker gets magnified by three orders of magnitude as it reaches the base of the whisker (Fig 11B). It is interesting to note that κ_i shifts the range of moment that is experienced by the whisker base resulting in a sign change of moment, and therefore might be partly responsible for the second bending mode of acceleration and curvature (cf. Fig. 11). Figure 11C shows the time series behavior of $\mathrm{M_{na}}$ at the tip and the base scaled appropriately the inverse relationship of

moments at tip and base can be readily appreciated. Using stick and slip event timestamps to event-triggered averaging of moment shows that during a stick event, moment builds up (Fig. 11D) and is released after a slip event. (Fig. 11E). In summary, these results suggest how ‘intrinsic curvature’ and ‘conical shape’ of the whisker may critically determine the stimulation of end organs of primary afferents at the follicle. They assure the generation of stick-slip events at the tip, convey them instantly to the follicle and substantially amplify the associated moment in the movement plane.

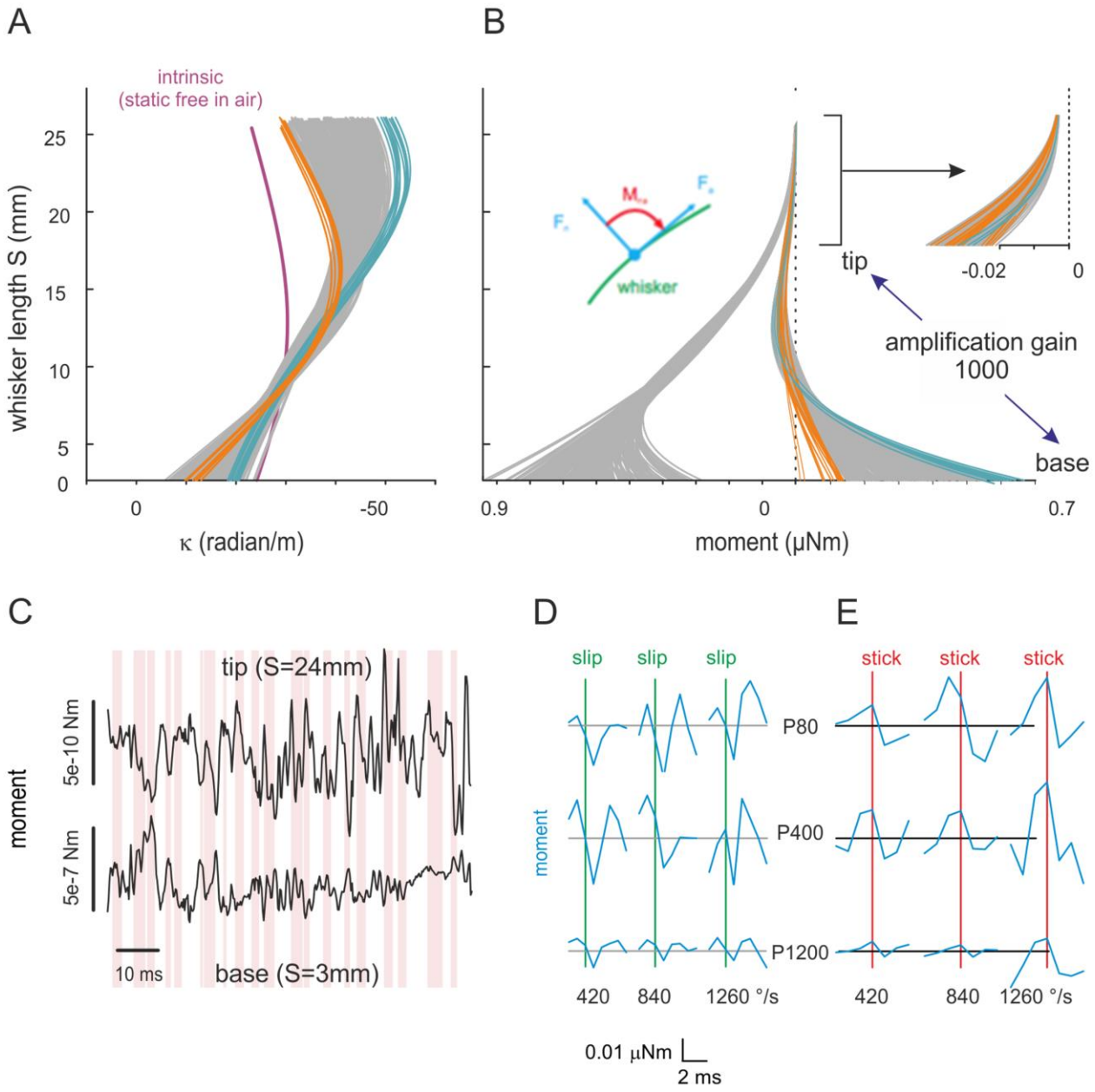

Figure 11. Amplification of moment from whisker tip to base. A) Curvature of whisker in contact with P80 (speed 420 °/s). The frames showing extreme curvature at the tip are colored to demonstrate a pivot of vibration at around 10 mm from the tip. B) Inset. Moment M_{na} at a certain point along the vibrissa acts in the plane defined by normal force F_n and the axial force F_a. At the tip moments are very small and negative (cf. inset). At the base they are amplified by approximately a factor 1000 and are positive. Again, the most extreme moments have been colored arbitrarily. The left bundle of moments depicts the raw data before subtraction of the intrinsic curvature. C) Moment traces across time (stick phases as given by all points below the velocity threshold (cf. Fig. 1D) are marked red) Note the difference of moment scale at tip vs.

base. D) Mean moment around slips. Nine correlograms applying three different sandpapers and three driving speeds are shown. E) Same as D for stick events.

Direct force measurements

To validate the indirect inference of moment from kinematic data I resorted to measurement of forces. To accomplish that I have used a highly sensitive piezo-resistive force sensor probe that is capable of measuring multiaxial forces in the Micro and Nano Newton range (Fig. 12A) (Kan et al., 2013). The whisker was fastened to the sensor by gluing the follicle side on the probe's cantilever. Sandpaper was attached to the inside arena of a rotating drum with the follicle as the center of the imaginary circle laid out by perimeter of the drum. As the rotation of hair with sensor was not possible due to the fragility of the sensor, the textured surface was moved instead against the stationary whisker. This set-up allowed me to measure the normal (F_n) and axial forces (F_a) at the whisker base (Fig. 12). In addition to force measurements, ultra-fast videography (9600 fps) was used to assess kinematics (acceleration) of one point of the shaft near the base (cf. Fig. 9; a_x, red in Fig. 12), as done before (cf. Fig. 4).

Interestingly, the force measurements revealed high absolute correlations between F_n, F_a, and a_x, with the forces being anti-correlated and a_x being correlated to F_n. The Pearson correlation coefficients were: $r_{F_n,a_x} = 0.9349$; $r_{F_a,a_x} = -0.9302$; $r_{F_n,F_a} = -0.9657$. Figure 5B plots the time series of the three measures for direct comparison. From these high correlations together with the finding that slip acceleration shows a high correlation to stick events (cf. Fig 11D) it follows that forces should relate to stick events as well. This expectation was met and is demonstrated in figure 12C. To summarize, the time series of acceleration at the base of the whisker estimated through analysis of videography provided a fair proxy to the time series of

forces acting on the whisker base. However, using acceleration as a proxy for these forces at the base is only a relative measure: the moment at the whisker base moment (and therefore presumably the forces as well) are subjected to the high amplification from the tip to the base, which is not the case for acceleration (cf. Figs. 9 and 11).

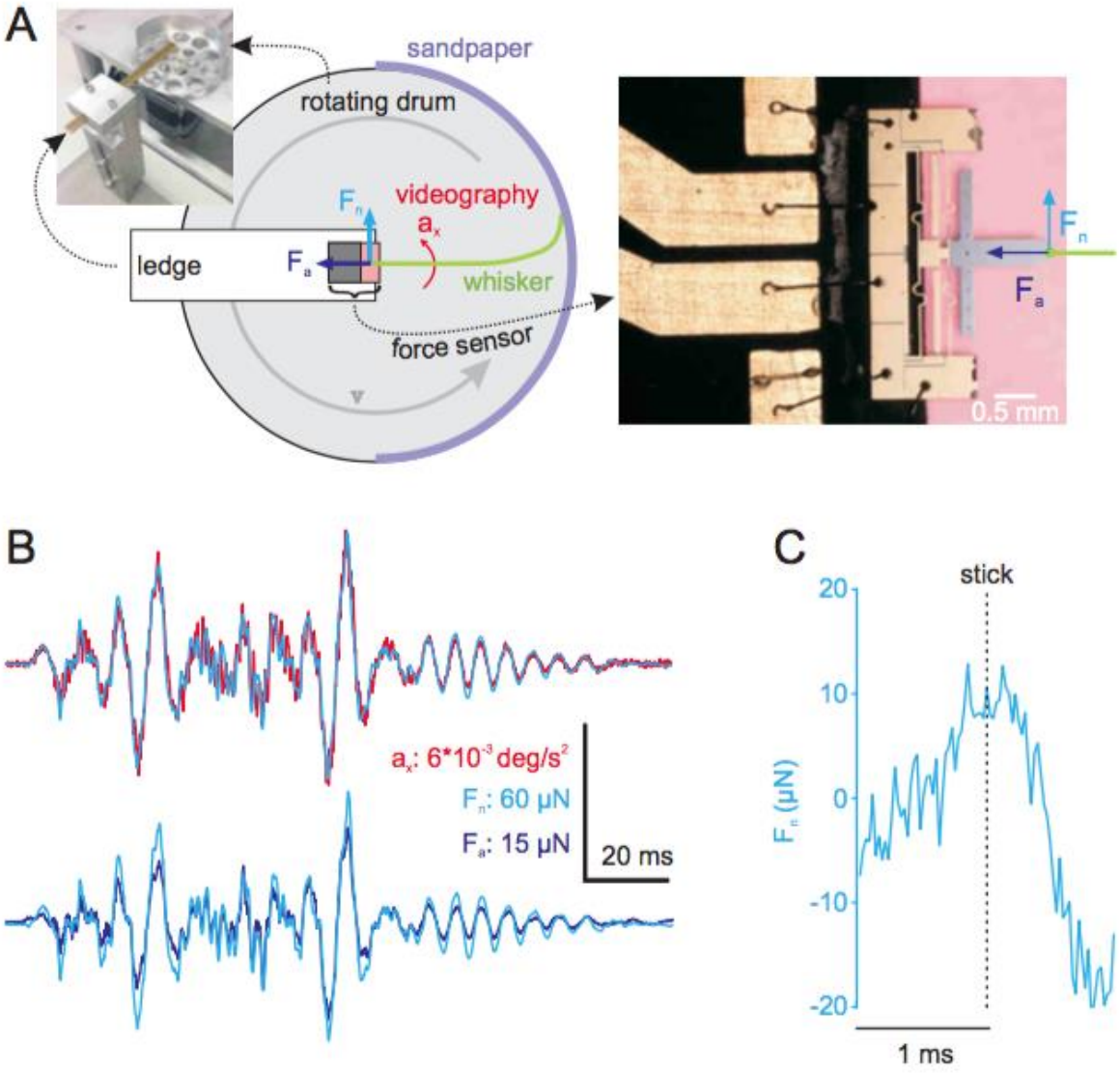

Figure 12. Direct force measurement. A) A highly sensitive piezo-resistive force sensor probe with the measurement range of multiaxial forces in the Micro and Nano Newton. The whisker was fastened to the sensor by gluing the follicle side on the probe's cantilever. Sandpaper was

attached to the inside arena of a rotating drum with the follicle as the center of the imaginary circle laid out by perimeter of the drum. B) The time series of the three measures (Normal force, Axial force, Acceleration) for direct comparison. Correlations between F_n, F_a, and a_x. C) Stick triggered average and force near the base.

Discussion

Ultrafast conveyance along the whisker beam and second order bending

The conveyance speed of vibrations from tip to follicle exceeded the frame-rate of 4 kHz of the ultra-fast videography, i.e. the conveyance time from tip to base was less than 0.25 ms. The conical shape of whiskers and the keratinous material suggest a high pliability of the whisker. While this is indeed the case for lateral deflections, normal to the beam, and mostly so toward the thin tip (Hires et al., 2013), it is also true that axial force, which is enacted by lateral tip movements via tip bending, meets with relative rigidity and inextensibility of the rod along its long axis. This fact is reflected by the observation of strong negative correlation between lateral deflections (a_x) and normal force (F_n) with axial force (F_a) (Fig. 12), and likely contributes to the ultra-fast conduction of vibrations down the whisker beam.

The inverse relationship of bending at tip and base was a surprising finding and is explained by a robust second order bending behavior of the whisker. Such behavior is non-trivial: its occurrence dependents on the fact that the whisker is intrinsically bent, even without load: Only after subtracting the intrinsic curvature, the moments acting on tip and base point in opposite directions (Fig. 11B). The location of the node of the 2nd bending mode likely depends on the conical shape of the beam. The typical movement direction in actively whisking species (like the rat studied here) has been associated with distinct innervation patterns most conspicuously at

the inner conical body of the follicle (Rice et al., 1986). The observed inverse relationship of tip vs. base deflection (and amplified moment; see next paragraph) will likely be instrumental to decipher the mechano-electrical transduction in those specifically formed and distributed end organs.

Amplification of moment

Time series of shaft acceleration and forces acting on the follicle showed very high correlations. This result is remarkable and its degree of reliance must be deemed very high in view of the fact that the two signals originate from two entirely independent measurements: whisker acceleration were acquired from videographic footage, while the follicular forces were assessed using the piezo-resistive force sensor. The result is potentially very useful, as it suggests that acceleration time series can serve as an excellent proxy for the normal force F_n acting on the base (and, after changing the sign, also to axial force F_a). It needs to be born in mind, however, that while acceleration may report well about relative dynamics of force, it will not be able to report about its absolute value. In view of the high amplification of dynamical variables observed here, this is still a serious limitation. Nevertheless, the found correspondence paves the way to use videographic measurements in behaving animals and report about the dynamics of forces acting on the follicle. In future approaches the assessment of absolute values of forces will be required. For these goals mathematical models need to be established that are able to convert kinematic into dynamic variables.

Transmission of frictional stick-slip movements

A strong negative correlation of F_n and F_a is intuitive. During stick phase of stick-slip events the whisker tip stays behind, and it is easy to see that it will give the base an axial pull from its fixture. As I defined F_a in direction of the follicle, it assumes negative values, while at the same time F_n builds up. During the slip phase these relationships are inversed. Comparing the measured F_n, F_a with the moment M_{na} inferred from curvature I could demonstrate that all three dynamic variables show significant and concerted dynamics with slips. It is commonly accepted that mechanosensitive membrane channels in tactile end organs pick up strains and forces (Delmas, Hao, & Rodat-Despoix, 2011; Hamill & Martinac, 2001; Kung, 2005). It is therefore important to demonstrate whether and how slips are represented in terms of dynamic variables. Together with the evidence that moments are greatly amplified on their way toward the whisker follicle, my present findings provide critical insight that slips are indeed represented robustly by forces and moments at the follicle, and that they therefore may have a high propensity to be transformed into precisely timed neuronal action potentials. This notion is supported by electrophysiological studies: single units in rat whisker-related primary somatosensory cortex respond to slip movements of whiskers in touch with sandpaper surfaces (Jadhav et al., 2009). More indirect evidence comes from studies employing broad band and pulsatile whisker deflections. Primary afferents preferentially encode local events (Chagas et al., 2013) and rats show the best change detection of series of pulsatile whisker deflections if details of pulse waveform rather than intensive variables change (Waiblinger, Brugger, & Schwarz, 2015).

Conclusion

In the current study, my goal was to find a mechanistic explanation of what happens as a single rat whisker engages in a moving contact with a textured surface - at the level of whisker dynamics. More specifically, I investigated how vibrations are conveyed from the tip to the base of a whisker. To accomplish that, I performed videographic measurements of the whisker kinematic profile and curvature, directly measured piezo-resistive forces at the whisker base. In the results I showed that, firstly, vibrations from the tip to base are conveyed at an ultrafast speed, and the second mode of bending is utilized. Secondly, the moment, which is a dynamic variable, is amplified by ~1000 times as it is conducted from the tip to the follicle of the whisker. Thirdly, I found that characteristic short-lived stick-slip frictional movements, featured prominently in dynamic signals, are transmitted down to the whisker base.

References

Andermann, M. L., Ritt, J., Neimark, M. A., & Moore, C. I. (2004). Neural correlates of vibrissa resonance; band-pass and somatotopic representation of high-frequency stimuli. *Neuron, 42*(3), 451-463.

Arabzadeh, E., Zorzin, E., & Diamond, M. E. (2005). Neuronal encoding of texture in the whisker sensory pathway. *PLoS Biol, 3*(1), e17. doi:10.1371/journal.pbio.0030017

Bensmaia, S., & Hollins, M. (2005). Pacinian representations of fine surface texture. *Percept Psychophys, 67*(5), 842-854.

Bensmaia, S. J., & Hollins, M. (2003). The vibrations of texture. *Somatosens Mot Res, 20*(1), 33-43. doi:10.1080/0899022031000083825

Bergmann Tiest, W. M. (2010). Tactual perception of material properties. *Vision Research, 50*(24), 2775-2782. doi:https://doi.org/10.1016/j.visres.2010.10.005

Bermejo, R., Houben, D., & Zeigler, H. P. (1998). Optoelectronic monitoring of individual whisker movements in rats. *J Neurosci Methods, 83*(2), 89-96.

Birdwell, J. A., Solomon, J. H., Thajchayapong, M., Taylor, M. A., Cheely, M., Towal, R. B., . . . Hartmann, M. J. (2007). Biomechanical models for radial distance determination by the rat vibrissal system. *J Neurophysiol, 98*(4), 2439-2455. doi:10.1152/jn.00707.2006

Bush, N. E., Solla, S. A., & Hartmann, M. J. (2016). Whisking mechanics and active sensing. *Curr Opin Neurobiol, 40*, 178-188. doi:10.1016/j.conb.2016.08.001

Carvell, G. E., & Simons, D. J. (1995). Task- and subject-related differences in sensorimotor behavior during active touch. *Somatosens Mot Res, 12*(1), 1-9.

Chagas, A. M., Theis, L., Sengupta, B., Stuttgen, M. C., Bethge, M., & Schwarz, C. (2013). Functional analysis of ultra high information rates conveyed by rat vibrissal primary afferents. *Front Neural Circuits, 7*, 190. doi:10.3389/fncir.2013.00190

Delmas, P., Hao, J., & Rodat-Despoix, L. (2011). *Molecular mechanisms of mechanotransduction in mammalian sensory neurons* (Vol. 12).

Ebara, S., Kumamoto, K., Matsuura, T., Mazurkiewicz, J. E., & Rice, F. L. (2002). Similarities and differences in the innervation of mystacial vibrissal follicle–sinus complexes in the rat and cat: A confocal microscopic study. *449*(2), 103-119. doi:10.1002/cne.10277

Gamzu, E., & Ahissar, E. (2001). Importance of temporal cues for tactile spatial- frequency discrimination. *J Neurosci, 21*(18), 7416-7427.

Gerdjikov, T. V., Bergner, C. G., & Schwarz, C. (2018). Global Tactile Coding in Rat Barrel Cortex in the Absence of Local Cues. *Cerebral Cortex, 28*(6), 2015-2027. doi:10.1093/cercor/bhx108

Gerdjikov, T. V., Bergner, C. G., Stuttgen, M. C., Waiblinger, C., & Schwarz, C. (2010). Discrimination of vibrotactile stimuli in the rat whisker system: behavior and neurometrics. *Neuron, 65*(4), 530-540. doi:10.1016/j.neuron.2010.02.007

Guic-Robles, E., Valdivieso, C., & Guajardo, G. (1989). Rats can learn a roughness discrimination using only their vibrissal system. *Behav Brain Res, 31*(3), 285-289.

Hafner, V. V., Fend, M., Lungarella, M., Pfeifer, R., Konig, P., & Kording, K. P. (2003). Optimal coding for naturally occurring whisker deflections. *Artificial Neural Networks and Neural Information Processing - Ican/Iconip 2003, 2714*, 805-812.

Hamill, O. P., & Martinac, B. (2001). Molecular Basis of Mechanotransduction in Living Cells. *81*(2), 685-740. doi:10.1152/physrev.2001.81.2.685

Hartmann, M. J., Johnson, N. J., Towal, R. B., & Assad, C. (2003). Mechanical characteristics of rat vibrissae: resonant frequencies and damping in isolated whiskers and in the awake behaving animal. *J Neurosci, 23*(16), 6510-6519.

Hipp, J., Arabzadeh, E., Zorzin, E., Conradt, J., Kayser, C., Diamond, M. E., & Konig, P. (2006). Texture signals in whisker vibrations. *J Neurophysiol, 95*(3), 1792-1799. doi:10.1152/jn.01104.2005

Hires, S. A., Pammer, L., Svoboda, K., & Golomb, D. (2013). Tapered whiskers are required for active tactile sensation. *Elife, 2*. doi:ARTN e01350

10.7554/eLife.01350

Hollins, M., & Risner, S. R. (2000). Evidence for the duplex theory of tactile texture perception. *Percept Psychophys, 62*(4), 695-705.

Jadhav, S. P., Wolfe, J., & Feldman, D. E. (2009). Sparse temporal coding of elementary tactile features during active whisker sensation. *Nat Neurosci, 12*(6), 792-800. doi:10.1038/nn.2328

Jones, L. M., Depireux, D. A., Simons, D. J., & Keller, A. (2004). Robust temporal coding in the trigeminal system. *Science, 304*(5679), 1986-1989. doi:10.1126/science.1097779

Kan, T., Takahashi, H., Binh-Khiem, N., Aoyama, Y., Takei, Y., Noda, K., . . . Shimoyama, I. (2013). Design of a piezoresistive triaxial force sensor probe using the sidewall doping method. *Journal of Micromechanics and Microengineering, 23*(3). doi:Artn 035027

10.1088/0960-1317/23/3/035027

Kung, C. (2005). A possible unifying principle for mechanosensation. *Nature, 436*(7051), 647-654. doi:10.1038/nature03896

LaMotte, R. H., & Mountcastle, V. B. (1975). Capacities of humans and monkeys to discriminate vibratory stimuli of different frequency and amplitude: a correlation between neural events and psychological measurements. *J Neurophysiol, 38*(3), 539-559. doi:10.1152/jn.1975.38.3.539

Lederman, S. J., Loomis, J. M., & Williams, D. A. (1982). The role of vibration in the tactual perception of roughness. *Percept Psychophys, 32*(2), 109-116.

Lederman, S. J. J. P., & Psychophysics. (1974). Tactile roughness of grooved surfaces: The touching process and effects of macro- and microsurface structure. *16*(2), 385-395. doi:10.3758/bf03203958

Manfredi, L. R., Saal, H. P., Brown, K. J., Zielinski, M. C., Dammann, J. F., 3rd, Polashock, V. S., & Bensmaia, S. J. (2014). Natural scenes in tactile texture. *J Neurophysiol, 111*(9), 1792-1802. doi:10.1152/jn.00680.2013

McGuire, L. M., Telian, G., Laboy-Juarez, K. J., Miyashita, T., Lee, D. J., Smith, K. A., & Feldman, D. E. (2016). Short Time-Scale Sensory Coding in S1 during Discrimination of Whisker Vibrotactile Sequences. *PLoS Biol, 14*(8), e1002549. doi:10.1371/journal.pbio.1002549

Mountcastle, V. B., LaMotte, R. H., & Carli, G. (1972). Detection thresholds for stimuli in humans and monkeys: comparison with threshold events in mechanoreceptive afferent nerve fibers innervating the monkey hand. *J Neurophysiol, 35*(1), 122-136. doi:10.1152/jn.1972.35.1.122

Neimark, M. A., Andermann, M. L., Hopfield, J. J., & Moore, C. I. (2003). Vibrissa resonance as a transduction mechanism for tactile encoding. *J Neurosci, 23*(16), 6499-6509.

Oladazimi, M., Brendel, W., & Schwarz, C. (2018). Biomechanical Texture Coding in Rat Whiskers. *Scientific Reports, 8*(1), 11139. doi:10.1038/s41598-018-29225-9

Persson, B. N. J., & Volokitin, A. I. (2006). Rubber friction on smooth surfaces. *European Physical Journal E, 21*(1), 69-80. doi:10.1140/epje/i2006-10045-9

Petersen, R. S., Brambilla, M., Bale, M. R., Alenda, A., Panzeri, S., Montemurro, M. A., & Maravall, M. (2008). Diverse and temporally precise kinetic feature selectivity in the VPm thalamic nucleus. *Neuron, 60*(5), 890-903. doi:10.1016/j.neuron.2008.09.041

Pinto, D. J., Brumberg, J. C., & Simons, D. J. (2000). Circuit dynamics and coding strategies in rodent somatosensory cortex. *J Neurophysiol, 83*(3), 1158-1166. doi:10.1152/jn.2000.83.3.1158

Prevost, A., Scheibert, J., & Debregeas, G. (2009). Effect of fingerprints orientation on skin vibrations during tactile exploration of textured surfaces. *Commun Integr Biol, 2*(5), 422-424.

Quist, B. W., Faruqi, R. A., & Hartmann, M. J. (2011). Variation in Young's modulus along the length of a rat vibrissa. *J Biomech, 44*(16), 2775-2781. doi:10.1016/j.jbiomech.2011.08.027

Ranade, S., Hangya, B., & Kepecs, A. (2013). Multiple Modes of Phase Locking between Sniffing and Whisking during Active Exploration. *Journal of Neuroscience, 33*(19), 8250-8256. doi:10.1523/Jneurosci.3874-12.2013

Ritt, J. T., Andermann, M. L., & Moore, C. I. (2008). Embodied information processing: vibrissa mechanics and texture features shape micromotions in actively sensing rats. *Neuron, 57*(4), 599-613. doi:10.1016/j.neuron.2007.12.024

Schwarz, C. (2016). The Slip Hypothesis: Tactile Perception and its Neuronal Bases. *Trends Neurosci, 39*(7), 449-462. doi:10.1016/j.tins.2016.04.008

Shadmehr, R., & MussaIvaldi, S. (2012). Biological Learning and Control: How the Brain Builds Representations, Predicts Events, and Makes Decisions. *Biological Learning and Control: How the Brain Builds Representations, Predicts Events, and Makes Decisions*, 1-388.

Skedung, L., Arvidsson, M., Chung, J. Y., Stafford, C. M., Berglund, B., & Rutland, M. W. (2013). Feeling small: exploring the tactile perception limits. *Sci Rep, 3*, 2617. doi:10.1038/srep02617

Stuttgen, M. C., Ruter, J., & Schwarz, C. (2006). Two psychophysical channels of whisker deflection in rats align with two neuronal classes of primary afferents. *J Neurosci, 26*(30), 7933-7941. doi:10.1523/JNEUROSCI.1864-06.2006

Stuttgen, M. C., & Schwarz, C. (2008). Psychophysical and neurometric detection performance under stimulus uncertainty. *Nature Neuroscience, 11*(9), 1091-1099. doi:10.1038/nn.2162

Stuttgen, M. C., & Schwarz, C. (2010). Integration of Vibrotactile Signals for Whisker-Related Perception in Rats Is Governed by Short Time Constants: Comparison of Neurometric and Psychometric Detection Performance. *Journal of Neuroscience, 30*(6), 2060-2069. doi:10.1523/Jneurosci.3943-09.2010

Taylor, M. M., & Lederman, S. J. (1975). Tactile Roughness of Grooved Surfaces - Model and Effect of Friction. *Perception & Psychophysics, 17*(1), 23-36. doi:Doi 10.3758/Bf03203993

Temereanca, S., & Simons, D. J. (2003). Local field potentials and the encoding of whisker deflections by population firing synchrony in thalamic barreloids. *J Neurophysiol, 89*(4), 2137-2145. doi:10.1152/jn.00582.2002

Towal, R. B., Quist, B. W., Gopal, V., Solomon, J. H., & Hartmann, M. J. (2011). The morphology of the rat vibrissal array: a model for quantifying spatiotemporal patterns of whisker-object contact. *PLoS Comput Biol, 7*(4), e1001120. doi:10.1371/journal.pcbi.1001120

Voges, D., Carl, K., Klauer, G. J., Uhlig, R., Schilling, C., Behn, C., & Witte, H. (2012). Structural Characterization of the Whisker System of the Rat. *Ieee Sensors Journal, 12*(2), 332-339. doi:10.1109/Jsen.2011.2161464

von Heimendahl, M., Itskov, P. M., Arabzadeh, E., & Diamond, M. E. (2007). Neuronal activity in rat barrel cortex underlying texture discrimination. *PLoS Biol, 5*(11), e305. doi:10.1371/journal.pbio.0050305

Waiblinger, C., Brugger, D., & Schwarz, C. (2015). Vibrotactile Discrimination in the Rat Whisker System is Based on Neuronal Coding of Instantaneous Kinematic Cues. *Cerebral Cortex, 25*(4), 1093-1106. doi:10.1093/cercor/bht305

Waiblinger, C., Brugger, D., Whitmire, C. J., Stanley, G. B., & Schwarz, C. (2015). Support for the slip hypothesis from whisker-related tactile perception of rats in a noisy environment. *Front Integr Neurosci, 9*, 53. doi:10.3389/fnint.2015.00053

Welker, W. I., Johnson, J. I., Jr., & Pubols, B. H., Jr. (1964). Some Morphological and Physiological Characteristics of the Somatic Sensory System in Raccoons. *Am Zool, 4*, 75-94.

Wolfe, J., Hill, D. N., Pahlavan, S., Drew, P. J., Kleinfeld, D., & Feldman, D. E. (2008). Texture coding in the rat whisker system: slip-stick versus differential resonance. *PLoS Biol, 6*(8), e215. doi:10.1371/journal.pbio.0060215